

Perfect Reconstruction Two-Channel Filter Banks on Arbitrary Graphs*

Junxia You and Lihua Yang[†]

School of Mathematics, Sun Yat-sen University, Guangzhou, China
Guangdong Province Key Laboratory of Computational Science

June 22, 2024

Abstract

This paper extends the existing theory of perfect reconstruction two-channel filter banks from bipartite graphs to non-bipartite graphs. By generalizing the concept of downsampling/upsampling we establish the frame of two-channel filter bank on arbitrary connected, undirected and weighted graphs. Then the equations for perfect reconstruction of the filter banks are presented and solved under proper conditions. Algorithms for designing orthogonal and biorthogonal banks are given and two typical orthogonal two-channel filter banks are calculated. The locality and approximation properties of such filter banks are discussed theoretically and experimentally.

Keywords: Graph signal processing, wavelets, two-channel filter banks, perfect reconstruction

1 Introduction

Graph signal processing (GSP) is an emerging field that studies signals defined on the vertices of a weighted graph: i.e. vertices connected by edges associated with non-negative weights [33, 23]. Weighted graphs provide a natural representation for data domain in many applications, such as the social networks, web information analysis, sensor networks and machine learning. The collections of samples on these graphs are termed as *graph signals*. For example, a social network can be modeled as a weighted graph by viewing the individual accounts as vertices, and the relationships between them as weighted edges. Then one can analyze the information of all the accounts in this network by using GSP tools. Similarly, in a sensor network, the sensors and the distances between each of them

*Supported by National Natural Science Foundation of China (Nos. 12171488, 11771458) and Guangdong Province Key Laboratory of Computational Science at the Sun Yat-sen University (2020B1212060032).

[†]Corresponding author

constitute a graph and the recorded data on the sensors defines a signal on the graph. In recent years, graph signal processing technology has been widely used [23, 13, 41, 15]. Graph signal processing aims at extending the well-developed theory and methods for analysis of signals defined in regular domains to those defined in irregular graph domains. There has been a lot of research in this field, including the Fourier transform of graph functions [30, 5, 40], graph sampling and reconstruction [19, 11, 38], approximation theory of graph functions [25, 12], graph wavelets and multiscale analysis [21, 2, 10, 6, 17, 9], and so on.

In many applications, a certain type of transform is applied to the original signal if it brings benefits in analysis in the transformed domain than in the original signal domain. And then the processing and analysis is performed on the coefficients of the transformed data. For processing of signals defined in the regular domains, transforms such as Fourier transform, windowed Fourier transform and wavelet transform have been developed. Among them, wavelet transform is particularly widely used for processing nonstationary signals because it catches the local information of the signal in both time and frequency domains. Naturally, people want to extend the theory and methods of wavelet analysis to the graph signal processing. However, due to the irregularity of graph structure, some traditional operations such as translation and dilation are difficult to establish in the graph settings. But people are still actively seeking ways to develop wavelet transforms on graphs.

In [3], Crovella and Kolaczyk constructed a series of simple functions on each neighbourhood of every vertex so that they are compactly supported and have zero integral over the entire vertex set. They refer to these functions as graph wavelet functions. Coifman and Maggioni proposed the concept of diffusion wavelets and use diffusion as a smoothing and scaling tool to enable coarse graining and multiscale analysis in [2]. Gavish et al. [9] first constructed multiscale wavelet-like orthonormal bases on hierarchical trees. They proved that function smoothness with respect to a metric induced by the tree is equivalent to approximate sparsity. Hammond et al. [10] constructed wavelet transforms in the graph domain based on the spectral graph theory, and they presented a fast Chebyshev polynomial approximation algorithm to improve efficiency. In follow-up work, they also built an almost tight wavelet frame based on the polynomial filters [35]. In [34], Shuman et al. proposed filters adapted to the distribution of graph Laplacian eigenvalues, leading to atoms with better discriminatory power. Inspired by the first-order spline filters in classical signal processing, Ekambaram et al. designed a class of critically sampled and perfect reconstruction spline wavelets, and was later extended to higher-order and exponential spline filters by Kotzagiannidis and Dragotti [8, 14]. In [21], Narang and Ortega designed perfect reconstruction two-channel filter banks on bipartite graphs based on the spectral folding phenomenon. For non-bipartite graphs, they proposed an algorithm that can decompose any graph into a series of bipartite subgraphs, thereby extending the design to arbitrary graphs. In the follow-up work [18], they constructed a class of biorthogonal wavelet filter banks on bipartite graphs, where all filters are polynomials in the Laplacian matrix.

When a non-bipartite graph is decomposed into several bipartite subgraphs, the signal processing on the original graph comes down to the signal processing on every bipartite subgraph. A challenging topic is: can we construct perfect reconstruction two-channel filter banks on non-bipartite graphs directly? Inspired by [21], by generalizing the concepts of downsampling and upsampling operations, we extend the construction of perfect reconstruction two-channel filter banks proposed in [21] to arbitrary connected, undirected, and weighted graphs in this paper. The locality and approximation property of such filter banks are discussed theoretically and experimentally.

The rest of the paper is organized as follows: Section 2 introduces some basic concepts including the graph Fourier transform, filters, downsampling and upsampling, and the two-channel filter banks. The related work [21] is also introduced briefly in this section to motivate our work, and the contribution of this paper is summarized at the end of this section. In section 3, the main theorem for constructing perfect reconstruction two-channel filter banks on arbitrary graphs is established. The generalized downsamplers/upsamplers are constructed and the perfect reconstruction equations for a two-channel filter bank are presented. Algorithms for designing orthogonal and biorthogonal filter banks are given and two typical orthogonal filter banks are designed. Finally, the locality and approximation property of the proposed filter banks are discussed theoretically and experimentally in Section 4.

2 Preliminary

2.1 Notations

We start by introducing the notations used throughout this paper. Vectors are denoted by lowercase boldfaced letters and matrices are denoted by uppercase boldfaced letters. The set of real numbers and the set of natural numbers are denoted as \mathbb{R} and \mathbb{N} respectively. For any $N, M \in \mathbb{N}$, the linear spaces of all the N -dimensional column vectors and all the matrices of order $N \times M$ are respectively denoted by \mathbb{R}^N and $\mathbb{R}^{N \times M}$. \mathbb{R}_+^N is the set of vectors in \mathbb{R}^N whose components are all non-negative. The i th component of a vector \mathbf{x} is denoted by x_i or $\mathbf{x}(i)$. The (i, j) -entry of matrix \mathbf{A} is denoted by $\mathbf{A}(i, j)$ or a_{ij} . Let $\mathbf{1}_N$ and $\mathbf{0}_N$ represent the vectors in \mathbb{R}^N whose components are all 1 and 0 respectively. \mathbf{I}_N stands for the identity matrix of order N . For $1 \leq i \leq N$, let \mathbf{e}_i be the i th column of \mathbf{I}_N . For any $x \in \mathbb{R}$, $[x]$ represents the largest integer not exceeding x .

Let $\mathcal{G} = (\mathcal{V}, \mathcal{E}, \mathbf{W})$ be a connected, undirected and weighted graph with neither loops nor multiple edges, where $\mathcal{V} = \{v_1, \dots, v_N\}$ is the set of vertices, \mathcal{E} is the set of edges, and $\mathbf{W} \in \mathbb{R}^{N \times N}$ is the adjacency matrix with its entry w_{ij} the nonnegative weight of the edge between the vertices v_i and v_j . A graph signal $f : \mathcal{V} \rightarrow \mathbb{R}$ is a function defined on the vertices of the graph. Once the vertex order is fixed, the graph signal can be written as a vector $\mathbf{f} := (f(v_1), \dots, f(v_N))^T \in \mathbb{R}^N$, where the i th component equals the value of f on v_i . In this paper, we will not distinguish the difference between f and \mathbf{f} if no confusion arises.

The superscript \top indicates the transpose operation. Function $\text{diag}(\cdot)$ maps a vector to a diagonal matrix, or a matrix to its diagonal. We denote by $\langle \mathbf{v}, \mathbf{u} \rangle$ the inner product of the vectors \mathbf{u} and \mathbf{v} in the Euclidean space \mathbb{R}^N . The induced norm is called 2-norm and denoted by $\|\mathbf{u}\|_2$. We adopt the following Dirichlet form to measure the oscillation of a graph signal \mathbf{f} on \mathcal{G} [33]:

$$S_2(\mathbf{f}) := \frac{1}{2} \sum_{i=1}^N \sum_{j=1}^N w_{ij} |\mathbf{f}(v_i) - \mathbf{f}(v_j)|^2. \quad (2.1)$$

It is easy to see that the larger the value of $S_2(\mathbf{f})$, the stronger the signal oscillates and vice versa.

2.2 Fourier Transform and Filters

The Laplacian matrix of a graph $\mathcal{G} = (\mathcal{V}, \mathcal{E}, \mathbf{W})$ is defined as $\mathbf{L} := \mathbf{D} - \mathbf{W}$, where \mathbf{D} is the diagonal degree matrix $\text{diag}(d_1, \dots, d_N)$ with elements $d_i = \sum_{j=1}^N w_{ij}$ [1]. As the matrix \mathbf{L} is real symmetric and positive semi-definite, there exists a set of orthonormal eigenvectors $\{\mathbf{u}_l\}_{l=1}^N$ and real eigenvalues $0 = \lambda_1 < \lambda_2 \leq \dots \leq \lambda_N$ such that $\mathbf{L} = \mathbf{U}\Lambda\mathbf{U}^\top$, where

$$\mathbf{U} := (\mathbf{u}_1, \dots, \mathbf{u}_N), \quad \Lambda := \text{diag}(\lambda_1, \dots, \lambda_N).$$

The set of the eigenvectors $\{\mathbf{u}_l\}_{l=1}^N$ are often viewed as the graph Fourier basis and \mathbf{U} is called the Fourier basis matrix. Using the Fourier basis, the graph Fourier transform and the inverse Fourier transform are defined respectively as [33]:

$$\hat{\mathbf{f}} := \mathbf{U}^\top \mathbf{f}, \quad \mathbf{f} = \mathbf{U} \hat{\mathbf{f}}, \quad \forall \mathbf{f} \in \mathbb{R}^N.$$

With the Laplacian matrix \mathbf{L} , the Dirichlet form (2.1) can be rewritten as

$$S_2(\mathbf{f}) = \mathbf{f}^\top \mathbf{L} \mathbf{f} = \hat{\mathbf{f}}^\top \Lambda \hat{\mathbf{f}} = \sum_{k=1}^N \lambda_k |\hat{\mathbf{f}}(k)|^2. \quad (2.2)$$

Since $S_2(\mathbf{u}_l) = \mathbf{u}_l^\top \mathbf{L} \mathbf{u}_l = \lambda_l$, $l = 1, \dots, N$, we have that $S_2(\mathbf{u}_1) \leq \dots \leq S_2(\mathbf{u}_N)$, which shows that the oscillation of the Fourier basis $\mathbf{u}_1, \dots, \mathbf{u}_N$ becomes stronger as the index l increases. In view of the above, the Dirichlet form $S_2(\mathbf{f})$ is regarded as the frequency of \mathbf{f} . We call the set $\sigma(\mathbf{L}) := \{\lambda_1 < \lambda_2 \leq \dots \leq \lambda_N\}$ the spectra of \mathbf{L} .

There are several ways to define the Fourier transform of graph signals. In addition to the above-mentioned definition of using the eigenvectors of the graph Laplacian matrix \mathbf{L} , it can also be defined as the eigenvectors of the normalized Laplacian $\mathcal{L} := \mathbf{D}^{-1/2} \mathbf{L} \mathbf{D}^{-1/2}$ or the adjacency matrix \mathbf{W} [21, 30, 31]. From the perspective of minimizing the ℓ^1 oscillation of signals, we proposed a new definition of the graph Fourier basis in [40], which is proved to have better sparsity. In general, a graph Fourier basis $\{\mathbf{u}_1, \dots, \mathbf{u}_N\}$ is actually a family

of graph signals, which constitute an orthonormal basis of the signal space \mathbb{R}^N . As the index l increases, the oscillation of \mathbf{u}_l intensifies, which can also be understood as a gradual increase in frequency in a sense.

Filtering is the modulation of the Fourier transform of a signal, that is,

$$\mathbf{f} \xrightarrow{\text{FT}} \hat{\mathbf{f}} \xrightarrow{\text{M}} \begin{pmatrix} h_1 \hat{\mathbf{f}}_1 \\ \vdots \\ h_N \hat{\mathbf{f}}_N \end{pmatrix} \xrightarrow{\text{IFT}} \mathbf{F}_h \mathbf{f},$$

or equivalently $\mathbf{F}_h = \mathbf{U} \text{diag}(\mathbf{h}) \mathbf{U}^\top$, where FT, IFT and M are the abbreviations of “Fourier transform”, “Inverse Fourier Transform” and “Modulation”. The vector $\mathbf{h} := (h_1, \dots, h_N)^\top$ used for frequency modulation is called the filter vector.

2.3 Downsampling and Uppersampling

Downsampling (or subsampling) is the process of reducing the sampling rate of a signal. In the classical signal processing, it is usually done by keeping the first sample and then every other n th sample after the first. In the well-known Mallat’s decomposition algorithm in wavelet analysis, the signal is downsampled by $n = 2$. In the graph signal processing, a downsampling operation can be defined by choosing a subset $\mathcal{V}_1 \subset \mathcal{V}$ such that all samples of signal \mathbf{f} whose indices are not in \mathcal{V}_1 are discarded [21]. That is,

$$A_{\mathcal{V}_1} : (f_1, \dots, f_N)^\top \mapsto (f_{i_1}, \dots, f_{i_m})^\top, \quad (2.3)$$

where $\mathcal{V}_1 = \{v_{i_1}, \dots, v_{i_m}\}$ is the downsampled subset and $A_{\mathcal{V}_1}$ is the corresponding downsampler. One can choose different subsets to define downsamplers according to different applications [32, 20, 38, 39].

To reconstruct the signal one needs to upsample the downsampled signal by inserting zeros to increase the sampling rate. This upsampler can be described as

$$B_{\mathcal{V}_1} : (f_{i_1}, \dots, f_{i_m})^\top \mapsto (\tilde{f}_1, \dots, \tilde{f}_N)^\top, \quad \text{where } \tilde{f}_j := \begin{cases} f_j & j \in \mathcal{V}_1 = \{i_1, \dots, i_m\}, \\ 0 & \text{otherwise} . \end{cases} \quad (2.4)$$

Then the overall downsampling then upsampling operation can be illustrated by

$$\mathbf{f} \rightarrow A_{\mathcal{V}_1} \mathbf{f} \rightarrow B_{\mathcal{V}_1} A_{\mathcal{V}_1} \mathbf{f}.$$

It is easy to verify that

$$A_{\mathcal{V}_1}^\top = B_{\mathcal{V}_1} = [\mathbf{e}_{i_1}, \dots, \mathbf{e}_{i_m}] \in \mathbb{R}^{N \times m}$$

and $B_{\mathcal{V}_1} A_{\mathcal{V}_1}$ is a diagonal matrix whose i th diagonal entry is 1 if $v_i \in \mathcal{V}_1$ and 0 otherwise, i.e.,

$$B_{\mathcal{V}_1} A_{\mathcal{V}_1} = \frac{1}{2}(\mathbf{I}_N + \mathbf{J}), \quad (2.5)$$

where \mathbf{J} is a diagonal matrix whose diagonal entries are given by

$$\mathbf{J}(k, k) = \begin{cases} 1 & v_k \in \mathcal{V}_1, \\ -1 & v_k \notin \mathcal{V}_1, \end{cases} \quad k = 1, \dots, N. \quad (2.6)$$

In the following section, we will define the generalized downsampler and upsampler as matrices $\mathbf{A} \in \mathbb{R}^{m \times N}$ and $\mathbf{B} \in \mathbb{R}^{N \times m}$ with $m < N$.

2.4 Two-Channel Filter Banks

A two-channel filter bank is shown in Figure 1. It consists of two lowpass filters \mathbf{F}_{h_0} and \mathbf{F}_{g_0} , two highpass filters \mathbf{F}_{h_1} and \mathbf{F}_{g_1} , two downsamplers $\mathbf{A}_L, \mathbf{A}_H$ and two upsamplers $\mathbf{B}_L, \mathbf{B}_H$. The filters \mathbf{F}_{h_0} and \mathbf{F}_{h_1} are called analysis filters, and the filters \mathbf{F}_{g_0} and \mathbf{F}_{g_1} are called synthesis filters. With a two-channel filter bank, the input signal \mathbf{x} is separated into two frequency bands, a low frequency band corresponding to the upper channel, and a high frequency band corresponding to the lower channel. After the downsampling operation, the signal may be encoded for transmission or storage, in which case the information may be lost. Perfect reconstruction, i.e., $\mathbf{y} = \mathbf{x}$, requires that the analysis bank be connected directly to the synthesis bank, that is, we immediately upsample the signal after the downsampling operation [37]. A flow chart is displayed in Figure 1. The whole process can be mathematically expressed as (2.7).

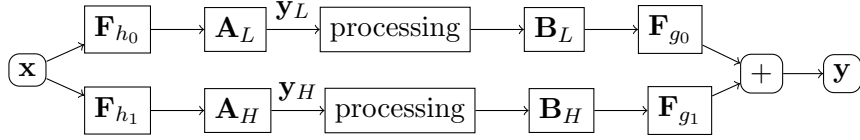


Figure 1: A two-channel filter bank.

$$\left\{ \begin{array}{l} \text{Input : } \mathbf{x} \\ \text{Analysis : } \begin{bmatrix} \mathbf{y}_L \\ \mathbf{y}_H \end{bmatrix} := \begin{bmatrix} \mathbf{A}_L \mathbf{F}_{h_0} \\ \mathbf{A}_H \mathbf{F}_{h_1} \end{bmatrix} \mathbf{x} \\ \text{Reconstruction : } \mathbf{y} := \begin{bmatrix} \mathbf{F}_{g_0} \mathbf{B}_L & \mathbf{F}_{g_1} \mathbf{B}_H \end{bmatrix} \begin{bmatrix} \mathbf{y}_L \\ \mathbf{y}_H \end{bmatrix} = \mathbf{F}_{g_0} \mathbf{B}_L \mathbf{y}_L + \mathbf{F}_{g_1} \mathbf{B}_H \mathbf{y}_H \\ \text{Output : } \mathbf{y} = \begin{bmatrix} \mathbf{F}_{g_0} \mathbf{B}_L & \mathbf{F}_{g_1} \mathbf{B}_H \end{bmatrix} \begin{bmatrix} \mathbf{A}_L \mathbf{F}_{h_0} \\ \mathbf{A}_H \mathbf{F}_{h_1} \end{bmatrix} \mathbf{x} \end{array} \right. \quad (2.7)$$

In practical applications, people need to construct different two-channel filter banks according to the application requirements. Mature mathematical theories on this subject

have been developed in classical signal processing [36]. In the settings of graph signal, it is still a challenging problem to design two-channel filter banks such that the following perfect reconstruction condition is satisfied:

$$\mathbf{F}_{g_0} \mathbf{B}_L \mathbf{A}_L \mathbf{F}_{h_0} + \mathbf{F}_{g_1} \mathbf{B}_H \mathbf{A}_H \mathbf{F}_{h_1} = \mathbf{I}_N. \quad (2.8)$$

2.5 Related Work

In [21], Narang and Ortega established the theory of perfect reconstruction two-channel filter banks for bipartite graph $\mathcal{G}_B = (\mathcal{V}, \mathcal{E})$, where the set of vertices \mathcal{V} can be divided into two disjoint subsets \mathcal{V}_1 and \mathcal{V}_2 such that each edge in \mathcal{E} connects a vertex in \mathcal{V}_1 to a vertex in \mathcal{V}_2 . The downsampler and upsampler in the lowpass channel are respectively chosen as $\mathbf{A}_L = A_{\mathcal{V}_1}$ and $\mathbf{B}_L = B_{\mathcal{V}_1}$, which are defined by (2.3) and (2.4). Similarly, the downsampler and upsampler in the highpass channel are respectively chosen as $\mathbf{A}_H = A_{\mathcal{V}_2}$ and $\mathbf{B}_H = B_{\mathcal{V}_2}$. According to (2.5), we have

$$\mathbf{B}_L \mathbf{A}_L = \frac{1}{2}(\mathbf{I}_N + \mathbf{J}_1), \quad \mathbf{B}_H \mathbf{A}_H = \frac{1}{2}(\mathbf{I}_N + \mathbf{J}_2),$$

where both \mathbf{J}_1 and \mathbf{J}_2 are diagonal matrix defined as follows:

$$\mathbf{J}_i(k, k) = \begin{cases} 1 & v_k \in \mathcal{V}_i, \\ -1 & v_k \notin \mathcal{V}_i, \end{cases} \quad k = 1, \dots, N, \quad i = 1, 2. \quad (2.9)$$

The eigenvectors of the normalized Laplacian matrix \mathcal{L} are served as the Fourier basis in [21]. Let $\sigma(\mathcal{L})$ be the corresponding spectrum set. By means of the equality $\mathbf{J}_1 + \mathbf{J}_2 = \mathbf{0}$, the perfect reconstruction condition (2.8) can be rewritten as

$$\underbrace{(\mathbf{F}_{g_0} \mathbf{F}_{h_0} + \mathbf{F}_{g_1} \mathbf{F}_{h_1})}_{\mathbf{T}_1} + \underbrace{(\mathbf{F}_{g_0} \mathbf{J}_1 \mathbf{F}_{h_0} + \mathbf{F}_{g_1} (-\mathbf{J}_1) \mathbf{F}_{h_1})}_{\mathbf{T}_2} = 2\mathbf{I}_N. \quad (2.10)$$

where

$$\mathbf{T}_1 = \sum_{\lambda \in \sigma(\mathcal{L})} (g_0(\lambda)h_0(\lambda) + g_1(\lambda)h_1(\lambda))\mathbf{P}_\lambda, \quad (2.11)$$

$$\mathbf{T}_2 = \sum_{\gamma, \lambda \in \sigma(\mathcal{L})} (g_0(\lambda)h_0(\gamma) - g_1(\lambda)h_1(\gamma))\mathbf{P}_\lambda \mathbf{J}_1 \mathbf{P}_\gamma. \quad (2.12)$$

where \mathbf{P}_λ is the orthogonal projector from \mathbb{R}^N to the eigen-subspace $V_\lambda := \text{span}\{\mathbf{u} | \mathcal{L}\mathbf{u} = \lambda\mathbf{u}\}$. For the bipartite graph \mathcal{G}_B , since

$$\lambda \in \sigma(\mathcal{L}) \iff 2 - \lambda \in \sigma(\mathcal{L}), \quad \mathbf{J}_1 \mathbf{P}_\lambda = \mathbf{P}_{2-\lambda} \mathbf{J}_1, \quad (2.13)$$

there holds that

$$\mathbf{T}_2 = \sum_{\lambda \in \sigma(\mathcal{L})} [g_0(\lambda)h_0(2-\lambda) - g_1(\lambda)h_1(2-\lambda)] \mathbf{P}_\lambda \mathbf{P}_{2-\lambda} \mathbf{J}_1.$$

Thus perfect reconstruction condition (2.10) is guaranteed by

$$\begin{cases} g_0(\lambda)h_0(\lambda) + g_1(\lambda)h_1(\lambda) = 2, \\ g_1(\lambda)h_1(2-\lambda) - g_0(\lambda)h_0(2-\lambda) = 0, \end{cases} \quad \forall \lambda \in \sigma(\mathcal{L}). \quad (2.14)$$

By setting $g_0(\lambda) = h_1(2-\lambda)$ and $g_1(\lambda) = h_0(2-\lambda)$, (2.14) can be simplified as

$$g_0(\lambda)h_0(\lambda) + g_0(2-\lambda)h_0(2-\lambda) = 2, \quad \forall \lambda \in \sigma(\mathcal{L}). \quad (2.15)$$

The resulting filter banks are said to be biorthogonal, which are studied in [18]. Furthermore, if $g_i(\lambda) = h_i(\lambda)$ for $i = 0, 1$, then (2.14) is equivalent to

$$|h_0(\lambda)|^2 + |h_1(\lambda)|^2 = 2, \quad \forall \lambda \in \sigma(\mathcal{L}).$$

The filter banks satisfying the equation are said to be orthogonal, which are studied in [21]. The technique for the construction is very skillful. However, it only applies to bipartite graphs due to the key condition (2.13). For non-bipartite graphs the authors of [21] proposed an approach, called Harary's decomposition, to decompose the graph into about $\lceil \log_2 K \rceil$ bipartite subgraphs, then the filter bank is built based on each bipartite graph. For more details, readers are referred to [21].

2.6 Our Contribution

In this paper, we extend the spectral folding property (2.13) and the perfect reconstruction condition (2.14) on bipartite graphs to arbitrary graphs. Specifically, for a given graph Fourier basis, we designed an orthogonal matrix \mathbf{Q} which plays the role of the above matrix \mathbf{J} , such that \mathbf{Q} and the projection matrix \mathbf{P}_λ satisfy a commutative equation similar to (2.13). Furthermore, we construct the generalized up/down-samplers based on \mathbf{Q} and propose the perfect reconstruction equations for the two-channel filter banks on arbitrary graphs. Under proper assumption, the general solutions of the equations are given. Theories on the approximation property and the locality of the filter banks are established. Finally, experiments for two special two-channel filter banks are conducted to verify the theoretical results.

3 Two-channel Filter Banks for Arbitrary Graphs

3.1 Two-channel Filter Banks Based on Generalized Samplers

In this section, we will construct the perfect reconstruction two-channel filter banks for arbitrary connected, weighted and undirected graphs. As discussed above, the condition

(2.13) is generally no longer valid, which makes it difficult to derive the perfect reconstruction condition (2.14) by requiring the matrix \mathbf{T}_2 defined in (2.12) to be zero. In order to overcome this inherent obstacle of non-bipartite graphs, we generalize the downsampler and upsampler defined by (2.3) and (2.4) to a pair of matrices $\mathbf{A} \in \mathbb{R}^{m \times N}$ and $\mathbf{B} \in \mathbb{R}^{N \times m}$ with $m \approx N/2$, and study the perfect reconstruction condition (2.8). That is, we hope to find proper $\mathbf{A}_L, \mathbf{A}_H, \mathbf{B}_L, \mathbf{B}_H$ and construct filters $\mathbf{F}_{h_0}, \mathbf{F}_{g_0}, \mathbf{F}_{h_1}, \mathbf{F}_{g_1}$ such that the following perfect reconstruction condition holds:

$$\mathbf{F}_{g_0} \mathbf{B}_L \mathbf{A}_L \mathbf{F}_{h_0} + \mathbf{F}_{g_1} \mathbf{B}_H \mathbf{A}_H \mathbf{F}_{h_1} = \mathbf{I}_N. \quad (3.1)$$

Inspired by the equality (2.5) in the case of bipartite graphs, we assume that the downsamplers $\mathbf{A}_L, \mathbf{A}_H$ and the upsamplers $\mathbf{B}_L, \mathbf{B}_H$ meet the following conditions:

$$\mathbf{B}_L \mathbf{A}_L = \frac{1}{2}(\mathbf{I}_N + \mathbf{Q}), \quad \mathbf{B}_H \mathbf{A}_H = \frac{1}{2}(\mathbf{I}_N - \mathbf{Q}), \quad (3.2)$$

where \mathbf{Q} is an orthogonal matrix to be determined.

For the sake of clearness of description, we introduce the following notations: A partition of the Fourier basis $\{\mathbf{u}_1, \dots, \mathbf{u}_N\}$ is a family of disjoint subsets $\{\mathcal{U}_\omega\}_{\omega \in \Omega}$ satisfying

$$\bigcup_{\omega \in \Omega} \mathcal{U}_\omega = \{\mathbf{u}_1, \dots, \mathbf{u}_N\}.$$

With this partition, any function $h : \Omega \rightarrow \mathbb{R}$ determines a filter vector $\mathbf{h} = (h_1, \dots, h_N)^\top$:

$$h_i := h(\omega), \quad \mathbf{u}_i \in \mathcal{U}_\omega, \quad i = 1, \dots, N.$$

Thus the corresponding filter \mathbf{F}_h can be expressed as

$$\mathbf{F}_h = \sum_{i=1}^N h_i \mathbf{u}_i \mathbf{u}_i^\top = \sum_{\omega \in \Omega} h(\omega) \sum_{\mathbf{u} \in \mathcal{U}_\omega} \mathbf{u} \mathbf{u}^\top = \sum_{\omega \in \Omega} h(\omega) \mathbf{P}_\omega,$$

where $\mathbf{P}_\omega := \sum_{\mathbf{u} \in \mathcal{U}_\omega} \mathbf{u} \mathbf{u}^\top$ is the orthogonal projector from \mathbb{R}^N to $\mathcal{X}_\omega := \text{span}(\mathcal{U}_\omega)$. For this reason, any function $h : \Omega \rightarrow \mathbb{R}$ is called a filter function associated with the partition.

Theorem 3.1. *Let $\{\mathcal{U}_\omega\}_{\omega \in \Omega}$ be a partition of the Fourier basis $\{\mathbf{u}_1, \dots, \mathbf{u}_N\}$ and \mathbf{Q} be an orthogonal matrix of order N satisfying*

$$\mathbf{Q} \mathcal{X}_\omega = \mathcal{X}_{\kappa(\omega)} \quad \text{for } \mathcal{X}_\omega := \text{span}(\mathcal{U}_\omega), \quad \forall \omega \in \Omega, \quad (3.3)$$

where $\kappa : \Omega \rightarrow \Omega$ is a bijection. Assume that $\mathbf{A}_L, \mathbf{A}_H, \mathbf{B}_L, \mathbf{B}_H$ are respectively downsamplers and upsamplers satisfying (3.2). Then (3.1) holds if the filter functions h_0, h_1, g_0, g_1 associated with the partition satisfy

$$\begin{cases} g_0(\omega)h_0(\omega) + g_1(\omega)h_1(\omega) = 2, \\ g_0(\kappa(\omega))h_0(\omega) = g_1(\kappa(\omega))h_1(\omega), \end{cases} \quad \forall \omega \in \Omega. \quad (3.4)$$

Proof. By inserting (3.2) into (3.1), the perfect reconstruction condition can be rewritten as

$$\mathbf{F}_{g_0}\mathbf{F}_{h_0} + \mathbf{F}_{g_1}\mathbf{F}_{h_1} + \mathbf{F}_{g_0}\mathbf{Q}\mathbf{F}_{h_0} - \mathbf{F}_{g_1}\mathbf{Q}\mathbf{F}_{h_1} = 2\mathbf{I}_N. \quad (3.5)$$

For any $\omega \in \Omega$, let $\{\mathbf{u}_{i_1}, \dots, \mathbf{u}_{i_k}\}$ be an orthonormal basis of \mathcal{X}_ω . Then $\{\mathbf{Q}\mathbf{u}_{i_1}, \dots, \mathbf{Q}\mathbf{u}_{i_k}\}$ is an orthonormal basis of $\mathcal{X}_{\kappa(\omega)}$. It is followed that the orthonormal projectors $\mathbf{P}_{\mathcal{X}_\omega} : \mathbb{C}^N \rightarrow \mathcal{X}_\omega$ and $\mathbf{P}_{\mathcal{X}_{\kappa(\omega)}} : \mathbb{C}^N \rightarrow \mathcal{X}_{\kappa(\omega)}$ can be respectively written as

$$\mathbf{P}_{\mathcal{X}_\omega} = \sum_{j=1}^k \mathbf{u}_{i_j} \mathbf{u}_{i_j}^\top, \quad \mathbf{P}_{\mathcal{X}_{\kappa(\omega)}} = \sum_{j=1}^k (\mathbf{Q}\mathbf{u}_{i_j})(\mathbf{Q}\mathbf{u}_{i_j})^\top,$$

which implies that $\mathbf{P}_{\mathcal{X}_{\kappa(\omega)}} = \mathbf{Q}\mathbf{P}_{\mathcal{X}_\omega}\mathbf{Q}^\top$. For any filter function associated with the partition: $h : \Omega \rightarrow \mathbb{R}$, we have

$$\mathbf{F}_{h \circ \kappa} = \sum_{\omega \in \Omega} h(\kappa(\omega))\mathbf{P}_{\mathcal{X}_\omega} = \mathbf{Q}^\top \left(\sum_{\omega \in \Omega} h(\kappa(\omega))\mathbf{P}_{\mathcal{X}_{\kappa(\omega)}} \right) \mathbf{Q} = \mathbf{Q}^\top \left(\sum_{\omega \in \Omega} h(\omega)\mathbf{P}_{\mathcal{X}_\omega} \right) \mathbf{Q} = \mathbf{Q}^\top \mathbf{F}_h \mathbf{Q},$$

i.e., $\mathbf{Q}\mathbf{F}_{h \circ \kappa} = \mathbf{F}_h \mathbf{Q}$. Consequently there holds

$$\mathbf{F}_{g_0}\mathbf{Q}\mathbf{F}_{h_0} - \mathbf{F}_{g_1}\mathbf{Q}\mathbf{F}_{h_1} = \mathbf{Q}(\mathbf{F}_{g_0 \circ \kappa}\mathbf{F}_{h_0} - \mathbf{F}_{g_1 \circ \kappa}\mathbf{F}_{h_1}).$$

Thus, (3.5) is equivalent to

$$\mathbf{F}_{g_0}\mathbf{F}_{h_0} + \mathbf{F}_{g_1}\mathbf{F}_{h_1} + \mathbf{Q}(\mathbf{F}_{g_0 \circ \kappa}\mathbf{F}_{h_0} - \mathbf{F}_{g_1 \circ \kappa}\mathbf{F}_{h_1}) = 2\mathbf{I}_N. \quad (3.6)$$

Since $\mathbf{P}_\omega \mathbf{P}_{\omega'} = \delta_{\omega, \omega'} \mathbf{P}_\omega$, where $\delta_{\omega, \omega'}$ is the Kronecker delta function, we have

$$\mathbf{F}_{g_0}\mathbf{F}_{h_0} = \sum_{\omega \in \Omega} \sum_{\omega' \in \Omega} g_0(\omega)h_0(\omega')\mathbf{P}_\omega \mathbf{P}_{\omega'} = \sum_{\omega \in \Omega} g_0(\omega)h_0(\omega)\mathbf{P}_\omega.$$

Similar results hold for $\mathbf{F}_{g_1}\mathbf{F}_{h_1}$, $\mathbf{F}_{g_0 \circ \kappa}\mathbf{F}_{h_0}$ and $\mathbf{F}_{g_1 \circ \kappa}\mathbf{F}_{h_1}$. Using $\sum_{\omega \in \Omega} \mathbf{P}_\omega = \mathbf{I}_N$, we conclude that (3.6) can be rewritten as

$$\sum_{\omega \in \Omega} [g_0(\omega)h_0(\omega) + g_1(\omega)h_1(\omega) - 2]\mathbf{P}_\omega + \mathbf{Q} \sum_{\omega \in \Omega} [g_0(\kappa(\omega))h_0(\omega) - g_1(\kappa(\omega))h_1(\omega)]\mathbf{P}_\omega = 0.$$

This equality is guaranteed by (3.4), obviously. The proof is complete. \blacksquare

If the graph is bipartite and the Fourier basis $\mathbf{u}_1, \dots, \mathbf{u}_N$ are the eigenvectors of the normalized Laplacian matrix \mathcal{L} then the conditions of Theorem 3.1 are satisfied. In fact, by computing the entries we can verify that the adjacency matrix \mathbf{W} satisfies $\mathbf{W}\mathbf{J}_1 + \mathbf{J}_1\mathbf{W} = \mathbf{0}$ for \mathbf{J}_1 defined by (2.9), which together with $\mathbf{J}_1\mathbf{D} = \mathbf{D}\mathbf{J}_1$ implies that $\mathcal{L}\mathbf{J}_1 = 2\mathbf{J}_1 - \mathbf{J}_1\mathcal{L}$. Hence, $\mathcal{L}\mathbf{u} = \lambda\mathbf{u}$ if and only if $\mathcal{L}\mathbf{J}_1\mathbf{u} = (2 - \lambda)\mathbf{J}_1\mathbf{u}$. That means, for any $\lambda \in \sigma(\mathcal{L})$,

$$\mathbf{J}_1\mathcal{X}_\lambda = \mathcal{X}_{\kappa(\lambda)}, \quad \text{with } \kappa : \sigma(\mathcal{L}) \rightarrow \sigma(\mathcal{L}), \quad \kappa(\lambda) := 2 - \lambda,$$

where $\sigma(\mathcal{L})$ is the spectra of \mathcal{L} and \mathcal{X}_λ is the eigen-space associated with λ . Furthermore, according to the definitions of $\{B_{\mathcal{V}_i}, A_{\mathcal{V}_i}\}_{i=1,2}$, we have

$$B_{\mathcal{V}_1}A_{\mathcal{V}_1} = \frac{1}{2}(\mathbf{I}_N + \mathbf{J}_1), \quad B_{\mathcal{V}_2}A_{\mathcal{V}_2} = \frac{1}{2}(\mathbf{I}_N - \mathbf{J}_1).$$

It is easy to verify that the conditions of Theorem 3.1 are satisfied for $\mathbf{Q} =: \mathbf{J}_1$, $\Omega := \sigma(\mathcal{L})$, $\kappa(\omega) = 2 - \omega$, the downsamplers $A_{\mathcal{V}_1}, A_{\mathcal{V}_2}$ defined by (2.3) and the uppersamplers $B_{\mathcal{V}_1}, B_{\mathcal{V}_2}$ defined by (2.4). By Theorem 3.1, we obtain the perfect reconstruction condition (3.4), which is exactly the (2.14) presented in [21].

The orthogonal matrix \mathbf{Q} satisfying $\mathbf{Q}\mathcal{X}_\lambda = \mathcal{X}_{\kappa(\lambda)}$ can be chosen as a diagonal matrix \mathbf{J}_1 for bipartite graphs. This fact no longer holds for non-bipartite graphs, no matter whether the Fourier transform is defined by the normalized or non-normalized Laplacian matrix, unless $\mathbf{Q} = \pm\mathbf{I}_N$. We give an example to illustrate this. Let us consider a graph with 4 vertices as shown in Figure 2, whose Laplacian matrix is given by

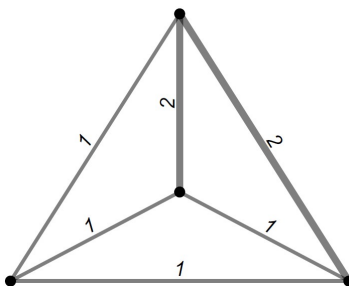


Figure 2: A graph of four vertices

$$\mathbf{L} = \begin{bmatrix} 4 & -1 & -1 & -2 \\ -1 & 3 & -1 & -1 \\ -1 & -1 & 4 & -2 \\ -2 & -1 & -2 & 5 \end{bmatrix}.$$

Then the eigendecomposition $\mathbf{L} = \mathbf{U}\mathbf{\Lambda}\mathbf{U}^\top$ gives the following eigenvectors and eigenvalues:

$$\mathbf{U} = \begin{bmatrix} -0.5000 & 0.2887 & 0.7071 & 0.4082 \\ -0.5000 & -0.8660 & 0.0000 & -0.0000 \\ -0.5000 & 0.2887 & -0.7071 & 0.4082 \\ -0.5000 & 0.2887 & 0 & -0.8165 \end{bmatrix}, \quad \mathbf{\Lambda} = \begin{bmatrix} 0 & 0 & 0 & 0 \\ 0 & 4 & 0 & 0 \\ 0 & 0 & 5 & 0 \\ 0 & 0 & 0 & 7 \end{bmatrix}.$$

Since the four numbers of each row of \mathbf{U} have different absolute values, there does not exist diagonal matrix \mathbf{Q} with diagonal entries ± 1 such that $\{\mathbf{Q}\mathbf{u}_i\}_{i=1}^4$ are still eigenvectors of \mathbf{L} . Similar result holds for normalized Laplacian, which shows that there is no diagonal matrix \mathbf{Q} with diagonal entries ± 1 that satisfies $\mathbf{Q}\mathcal{X}_\lambda = \mathcal{X}_{\kappa(\lambda)}$.

For any $\omega \in \Omega$, let \mathbf{U}_ω be the submatrix of \mathbf{U} whose columns constitute a basis of \mathcal{X}_ω . Then the condition (3.3) is equivalent to the existence of orthogonal matrices $\{A_\omega\}_{\omega \in \Omega}$ such that

$$\mathbf{Q}\mathbf{U}_\omega = \mathbf{U}_{\kappa(\omega)}A_\omega, \quad \omega \in \Omega.$$

Let $\Omega := \{\omega_1, \dots, \omega_n\}$. Then

$$\mathbf{Q}[\mathbf{U}_{\omega_1}, \dots, \mathbf{U}_{\omega_n}] = [\mathbf{Q}\mathbf{U}_{\omega_1}, \dots, \mathbf{Q}\mathbf{U}_{\omega_n}] = [\mathbf{U}_{\kappa(\omega_1)}, \dots, \mathbf{U}_{\kappa(\omega_n)}]A_\Omega \text{ with } A_\Omega := \begin{bmatrix} A_{\omega_1} & & \\ & \ddots & \\ & & A_{\omega_n} \end{bmatrix}.$$

Let Φ be a block permutation and \mathbf{P} be a permutation satisfying

$$[\mathbf{U}_{\kappa(\omega_1)}, \dots, \mathbf{U}_{\kappa(\omega_n)}] = [\mathbf{U}_{\omega_1}, \dots, \mathbf{U}_{\omega_n}]\Phi, \quad [\mathbf{U}_{\omega_1}, \dots, \mathbf{U}_{\omega_n}] = \mathbf{U}\mathbf{P}.$$

Then

$$\mathbf{Q}\mathbf{U} = \mathbf{U}\mathbf{P}\Phi A_\Omega \mathbf{P}^\top. \quad (3.7)$$

As a special case, let us consider the following partition of the Fourier basis:

$$\mathcal{U}_i = \text{span}\{\mathbf{u}_i\}, \quad i \in \Omega := \{1, \dots, N\},$$

and the orthogonal matrices $\{A_{\omega_k}\}$ are positive definite. In this case, we have that $A_\Omega = \mathbf{I}_N$ and the condition (3.7) can be rewritten as $\mathbf{Q}\mathbf{U} = \mathbf{U}\Phi$, where Φ is a permutation matrix of order N . By Theorem 3.1, we have the following corollary.

Corollary 3.2. *Let \mathbf{U} be a Fourier basis matrix and \mathbf{Q} an orthogonal matrix of order N satisfying*

$$\mathbf{Q}\mathbf{U} = \mathbf{U}\Phi \quad (3.8)$$

for a permutation matrix Φ . Assume $\mathbf{A}_L, \mathbf{A}_H, \mathbf{B}_L, \mathbf{B}_H$ are respectively downsamplers and upsamplers satisfying (3.2). Then the perfect reconstruction condition (3.1) holds if

$$\mathbf{g}_0 \odot \mathbf{h}_0 + \mathbf{g}_1 \odot \mathbf{h}_1 = 2\mathbf{1}_N, \quad (\Phi^\top \mathbf{g}_0) \odot \mathbf{h}_0 = (\Phi^\top \mathbf{g}_1) \odot \mathbf{h}_1, \quad (3.9)$$

where \odot stands for the Hadamard product.

Hereafter, unless otherwise noted, we will use the eigenvectors of the non-normalized Laplacian matrix as the Fourier basis.

3.2 Construction of Two-channel Filter Banks for Arbitrary Graphs

3.2.1 Construction of \mathbf{Q}

In this section, we will use Corollary 3.2 to construct a perfect reconstruction two-channel filter bank. To do this, we need to construct an orthogonal matrix \mathbf{Q} satisfying (3.8) and proper downsamplers $\mathbf{A}_L, \mathbf{A}_H$ and upsamplers $\mathbf{B}_L, \mathbf{B}_H$ with sizes $\mathbf{A}_L, \mathbf{B}_L^\top \in \mathbb{R}^{m \times N}$ and $\mathbf{A}_H, \mathbf{B}_H^\top \in \mathbb{R}^{(N-m) \times N}$ for $m \approx N/2$ such that (3.2) holds. Generally, the downsamplers $\mathbf{A}_L, \mathbf{A}_H$ are supposed to be full row rank and the upsamplers $\mathbf{B}_L, \mathbf{B}_H$ to be full column rank. According to (3.2), the ranks of $\mathbf{I} + \mathbf{Q}$ and $\mathbf{I} - \mathbf{Q}$ should be approximately equal to $N/2$. Since $\mathbf{I} \pm \mathbf{Q} = \mathbf{U}(\mathbf{I} \pm \Phi)\mathbf{U}^\top$, the problem turns into finding a permutation matrix Φ such that $\text{rank}(\mathbf{I} \pm \Phi) \approx N/2$.

In the construction of the samplers in Section 3.2.2, the eigenvalues of the matrix Φ are required to be real. For this reason, the matrix Φ is always assumed to be symmetric in the rest of this paper.

Lemma 3.3. *Let Φ be a symmetric permutation matrix of order N . Then its eigenvalues are 1 or -1 , and the ranks of $\mathbf{I} \pm \Phi$ and the trace of Φ are given by*

$$\text{rank}(\mathbf{I} + \Phi) = m, \quad \text{rank}(\mathbf{I} - \Phi) = N - m, \quad \text{tr}(\Phi) = 2m - N,$$

where m is the algebraic multiplicity of eigenvalue 1 of Φ .

Proof. Let λ be an eigenvalue of Φ , then there is a unit vector \mathbf{x} such that $\Phi\mathbf{x} = \lambda\mathbf{x}$. Calculate the 2-norms of the vectors on both sides we get $|\lambda| = \|\Phi\mathbf{x}\|_2 = \|\mathbf{x}\|_2 = 1$, which yields $\lambda = \pm 1$. Therefore, Φ has the following Jordan decomposition:

$$\Phi = \mathbf{P} \begin{bmatrix} \mathbf{J}_1 & \\ & \mathbf{J}_{-1} \end{bmatrix} \mathbf{P}^{-1},$$

where \mathbf{P} is an invertible matrix, $\mathbf{J}_1, \mathbf{J}_{-1}$ are the Jordan matrices associated to the eigenvalues 1 and -1 . Let m be the order of \mathbf{J}_1 . Since

$$\mathbf{I} + \Phi = \mathbf{P} \begin{bmatrix} \mathbf{I}_m + \mathbf{J}_1 & \\ & \mathbf{I}_{N-m} + \mathbf{J}_{-1} \end{bmatrix} \mathbf{P}^{-1}, \quad \mathbf{I} - \Phi = \mathbf{P} \begin{bmatrix} \mathbf{I}_m - \mathbf{J}_1 & \\ & \mathbf{I}_{N-m} - \mathbf{J}_{-1} \end{bmatrix} \mathbf{P}^{-1},$$

we have $\text{rank}(\mathbf{I} + \Phi) = m$ and $\text{rank}(\mathbf{I} - \Phi) = N - m$.

Finally, it is easy to see that $\text{tr}(\Phi) = m - (N - m) = 2m - N$. ■

According to Lemma 3.3, we need to construct a symmetric permutation matrix Φ whose eigenvalue 1 has algebraic multiplicity $m \approx N/2$. That means the trace of Φ should be close to 0. It is easy to see that the following matrix

$$\Phi := [\mathbf{e}_N, \dots, \mathbf{e}_1] = \begin{bmatrix} & & & 1 \\ & & & \\ & & \ddots & \\ & & & \\ 1 & & & \end{bmatrix} \in \mathbb{R}^{N \times N} \quad (3.10)$$

satisfies our requirement since its trace is either 0 or 1. In this case, the algebraic multiplicity of 1 and -1 are respectively $\lfloor (N+1)/2 \rfloor$ and $\lfloor N/2 \rfloor$, both are approximately $N/2$.

3.2.2 Construction of Generalized Sampling Matrices

As discussed in Section 3.2.1, \mathbf{Q} can be chosen as $\mathbf{U}\Phi\mathbf{U}^\top$ where Φ is defined by (3.10). It is easy to see that (3.8) holds. According to Corollary 3.2, as long as \mathbf{Q} satisfies (3.2), i.e.,

$$\mathbf{B}_L\mathbf{A}_L = \frac{1}{2}(\mathbf{I}_N + \mathbf{Q}), \quad \mathbf{B}_H\mathbf{A}_H = \frac{1}{2}(\mathbf{I}_N - \mathbf{Q})$$

with downsamplers $\mathbf{A}_L, \mathbf{A}_H$ and upsamplers $\mathbf{B}_L, \mathbf{B}_H$, the perfect reconstruction two-channel filter bank can be obtained by solving the filter equations (3.9). In the rest of this section, we focus on the construction of $\mathbf{A}_L, \mathbf{A}_H$ and $\mathbf{B}_L, \mathbf{B}_H$ that satisfy (3.2).

Let

$$\begin{cases} r := \lfloor \frac{N}{2} \rfloor, \\ s := \lceil \frac{N+1}{2} \rceil, \end{cases} \quad \Phi_r := \begin{bmatrix} & & 1 \\ & \cdot & \\ 1 & & \end{bmatrix} \in \mathbb{R}^{r \times r}.$$

It is easy to see that $r + s = N$.

(1) If N is an even number, then

$$\mathbf{I}_N + \Phi = \begin{bmatrix} \mathbf{I}_r & \Phi_r \\ \Phi_r & \mathbf{I}_r \end{bmatrix} = \mathbf{P}_0\mathbf{P}_0^\top, \quad \mathbf{I}_N - \Phi = \begin{bmatrix} \mathbf{I}_r & -\Phi_r \\ -\Phi_r & \mathbf{I}_r \end{bmatrix} = \mathbf{P}_1\mathbf{P}_1^\top,$$

where

$$\mathbf{P}_0 := \begin{bmatrix} \mathbf{I}_r \\ \Phi_r \end{bmatrix}, \quad \mathbf{P}_1 := \begin{bmatrix} \mathbf{I}_r \\ -\Phi_r \end{bmatrix} \quad (3.11)$$

(2) If N is an odd number, similarly we have

$$\mathbf{I}_N + \Phi = \begin{bmatrix} \mathbf{I}_r & \mathbf{0} & \Phi_r \\ \mathbf{0} & 2 & \mathbf{0} \\ \Phi_r & \mathbf{0} & \mathbf{I}_r \end{bmatrix} = \mathbf{P}_0\mathbf{P}_0^\top, \quad \mathbf{I}_N - \Phi = \begin{bmatrix} \mathbf{I}_r & \mathbf{0} & -\Phi_r \\ \mathbf{0} & 0 & \mathbf{0} \\ -\Phi_r & \mathbf{0} & \mathbf{I}_r \end{bmatrix} = \mathbf{P}_1\mathbf{P}_1^\top,$$

where

$$\mathbf{P}_0 := \begin{bmatrix} \mathbf{I}_r & \mathbf{0} \\ \mathbf{0} & \sqrt{2} \\ \Phi_r & \mathbf{0} \end{bmatrix}, \quad \mathbf{P}_1 := \begin{bmatrix} \mathbf{I}_r \\ \mathbf{0} \\ -\Phi_r \end{bmatrix}. \quad (3.12)$$

In summary, no matter whether N is even or odd, there always exist matrices $\mathbf{P}_0 \in \mathbb{R}^{N \times s}$ and $\mathbf{P}_1 \in \mathbb{R}^{N \times r}$ such that

$$\mathbf{I}_N + \Phi = \mathbf{P}_0\mathbf{P}_0^\top, \quad \mathbf{I}_N - \Phi = \mathbf{P}_1\mathbf{P}_1^\top.$$

which leads to

$$\begin{aligned} \frac{1}{2}(\mathbf{I}_N + \mathbf{Q}) &= \left(\frac{1}{\sqrt{2}}\mathbf{U}\mathbf{P}_0\right)\left(\frac{1}{\sqrt{2}}\mathbf{U}\mathbf{P}_0\right)^\top =: \mathbf{B}_L\mathbf{A}_L, \\ \frac{1}{2}(\mathbf{I}_N - \mathbf{Q}) &= \left(\frac{1}{\sqrt{2}}\mathbf{U}\mathbf{P}_1\right)\left(\frac{1}{\sqrt{2}}\mathbf{U}\mathbf{P}_1\right)^\top =: \mathbf{B}_H\mathbf{A}_H. \end{aligned}$$

where

$$\mathbf{A}_L = \mathbf{B}_L^\top = \frac{1}{\sqrt{2}} \mathbf{U}_1 \mathbf{P}_0^\top \mathbf{U}^\top, \quad \mathbf{A}_H = \mathbf{B}_H^\top = \frac{1}{\sqrt{2}} \mathbf{P}_1^\top \mathbf{U}^\top \quad (3.13)$$

and \mathbf{U}_1 is an orthogonal matrix of order s , which will be explained and determined in the next section.

3.2.3 Graph Reduction

In the classical two-channel subband filtering scheme, an incoming signal $\mathbf{x}^{(0)}$ is convolved with a lowpass filter \mathbf{h}_0 and a highpass filter \mathbf{h}_1 , respectively. Then the two resulting signals are downsampled by taking the samples in turn to produce two signals $\mathbf{x}^{(1)}$ and $\mathbf{z}^{(1)}$ of half size of $\mathbf{x}^{(0)}$. They are respectively viewed as a coarser approximation and a difference between $\mathbf{x}^{(0)}$ and $\mathbf{x}^{(1)}$ since the filter \mathbf{h}_0 removes the high frequency components of $\mathbf{x}^{(0)}$ while \mathbf{h}_1 preserves the high frequency components. The coarser approximation $\mathbf{x}^{(1)}$, as a short one-dimensional signal, can be further repeatedly decomposed to produce coarser approximations, as illustrated by Figure 3 .

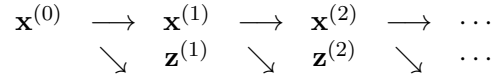


Figure 3: Mallat's decomposition

As described in Section 2.4, through a two-channel filter bank, a graph signal \mathbf{x} can be decomposed into two shorter vectors: a coarse approximation \mathbf{y}_L and a details part \mathbf{y}_H which contains the information about the difference between \mathbf{x} and \mathbf{y}_L . To further decompose \mathbf{y}_L into a coarser approximation of \mathbf{x} in the next level, we need to equip \mathbf{y}_L with a reduced graph that has a similar adjacency relationship to the original graph. This process of constructing a reduced graph is called graph reduction.

There are mainly two types of graph reduction. One is to select a subset of vertices of the original graph followed by re-wiring. The other is to aggregate some vertices into a new vertex followed by re-wiring. There are some works about graph reduction such as [29], [28, 7, 16], [27]. In this paper, we use the graph coarsening method proposed by [16]. Given a graph Laplacian $\mathbf{L} \in \mathbb{R}^{N \times N}$ and a number $s \approx N/2$, the Laplacian \mathbf{L}_1 of a graph \mathcal{G}_1 with s vertices and similar structure to \mathcal{G} can be constructed. Suppose the eigendecomposition of \mathbf{L}_1 is

$$\mathbf{L}_1 = \mathbf{U}_1 \Lambda_1 \mathbf{U}_1^\top.$$

Then, with \mathbf{U}_1 the samplers \mathbf{A}_L and \mathbf{B}_L are determined by (3.13).

3.2.4 Construction of Filters

Let us turn to the filter equation (3.9), i.e.

$$\begin{cases} \mathbf{g}_0(k)\mathbf{h}_0(k) + \mathbf{g}_1(k)\mathbf{h}_1(k) = 2, \\ \mathbf{g}_0(N+1-k)\mathbf{h}_0(k) = \mathbf{g}_1(N+1-k)\mathbf{h}_1(k), \end{cases} \quad k = 1, \dots, N.$$

For simplicity, we consider the following special filter bank:

$$\mathbf{g}_0(k) = \mathbf{h}_1(N+1-k), \quad \mathbf{g}_1(k) = \mathbf{h}_0(N+1-k), \quad k = 1, \dots, N.$$

Under these assumptions, Equation (3.9) is equivalent to

$$\mathbf{h}_0(k)\mathbf{g}_0(k) + \mathbf{h}_0(N+1-k)\mathbf{g}_0(N+1-k) = 2, \quad k = 1, \dots, N. \quad (3.14)$$

It is interesting to note that, Equation (3.14) looks like the perfect reconstruction equation of the classical biorthogonal wavelet bases [4]:

$$\overline{m_0(\xi)}\tilde{m}_0(\xi) + \overline{m_0(\xi + \pi)}\tilde{m}_0(\xi + \pi) = 1.$$

Thus, we refer to a filter bank $\{\mathbf{h}_0, \mathbf{g}_0, \mathbf{h}_1, \mathbf{g}_1\}$ satisfying (3.14) as a biorthogonal filter bank. Let $\mathbf{f}(k) := \mathbf{h}_0(k)\mathbf{g}_0(k)$. Then (3.14) can be rewritten as

$$\mathbf{f}(k) + \mathbf{f}(N+1-k) = 2, \quad k = 1, \dots, N. \quad (3.15)$$

The general solution of (3.15) is:

$$\mathbf{f}(N+1-k) = 2 - \mathbf{f}(k), \quad k = 1, \dots, s,$$

where $\mathbf{f}(1), \dots, \mathbf{f}(r)$ are free variables and $\mathbf{f}(s) = 1$ if N is an odd number. With \mathbf{f} , the vectors \mathbf{h}_0 and \mathbf{g}_0 can be solved from $\mathbf{h}_0 \odot \mathbf{g}_0 = \mathbf{f}$, i.e.,

$$\mathbf{h}_0(k)\mathbf{g}_0(k) = \mathbf{f}(k), \quad k = 1, \dots, N.$$

Particularly, if the analysis filters and the synthesis filters are the same, that is,

$$\mathbf{h}_0(k) = \mathbf{g}_0(k) = \sqrt{\mathbf{f}(k)}, \quad k = 1, \dots, N,$$

then the filter bank is said to be orthogonal. In this case, since $\mathbf{f}(k) = |\mathbf{h}_0(k)|^2 \geq 0$, we have

$$0 \leq \mathbf{f}(k) \leq 2, \quad k = 1, \dots, s.$$

In Section 4.1.1 we will talk about the locality of the filter, where a filter vector \mathbf{h} is desired to be expressed as or approximated by a polynomial in $\lambda \in \sigma(\mathbf{L})$. For this purpose, \mathbf{h} is assumed to satisfy

$$\lambda_i = \lambda_j \implies h_i = h_j \quad \text{and} \quad h_{N+1-i} = h_{N+1-j}, \quad \forall 1 \leq i < j \leq N, \quad \lambda_i, \lambda_j \in \sigma(\mathbf{L}).$$

Under this assumption we propose the following algorithm to construct a perfect reconstruction orthogonal filter bank from given parameters $\{y_i\}_{i=1}^s$.

Algorithm 3.1. Let $0 = \lambda_1 < \lambda_2 \leq \dots \leq \lambda_N$ be all the eigenvalues of the graph Laplacian \mathbf{L} and $r := \lfloor \frac{N}{2} \rfloor$, $s := \lfloor \frac{N+1}{2} \rfloor$.

1. Choose $2 = y_1 \geq \dots \geq y_s \geq 1$ and $y_s = 1$ for odd N satisfying

$$\lambda_i = \lambda_j \text{ or } \lambda_{N+1-i} = \lambda_{N+1-j} \implies y_i = y_j, \quad i, j = 1, \dots, s. \quad (3.16)$$

2. Set $y_{N+1-i} := 2 - y_i$, $i = 1, \dots, s$.
3. For $i = 1, \dots, N$, set $\mathbf{g}_0(i) = \mathbf{h}_0(i) = \sqrt{y_i}$ and $\mathbf{g}_1(i) = \mathbf{h}_1(i) := \mathbf{g}_0(N+1-i)$.
4. Output the orthogonal filter bank: $\{\mathbf{h}_0, \mathbf{g}_0, \mathbf{h}_1, \mathbf{g}_1\}$.

3.2.5 Mallat's Decomposition Algorithm

As shown in Figure 1, the input signal $\mathbf{x}^{(0)}$ is filtered to produce $\mathbf{F}_{h_0}\mathbf{x}^{(0)}$ and $\mathbf{F}_{h_1}\mathbf{x}^{(0)}$, which are further downsampled by \mathbf{A}_L and \mathbf{A}_H to produce the following two shorter signals:

$$\mathbf{x}^{(1)} := \mathbf{A}_L \mathbf{F}_{h_0} \mathbf{x}^{(0)}, \quad \mathbf{z}^{(1)} := \mathbf{A}_H \mathbf{F}_{h_1} \mathbf{x}^{(0)}, \quad (3.17)$$

where $\mathbf{A}_L, \mathbf{A}_H$ are defined by (3.13), namely,

$$\mathbf{A}_L = \frac{1}{\sqrt{2}} \mathbf{U}_1 \mathbf{P}_0^\top \mathbf{U}^\top, \quad \mathbf{A}_H = \frac{1}{\sqrt{2}} \mathbf{P}_1^\top \mathbf{U}^\top.$$

where \mathbf{P}_0 and \mathbf{P}_1 are designed according to (3.11) and (3.12).

According to Equation (3.1) for perfect reconstruction, we have

$$\mathbf{x}^{(0)} = \mathbf{F}_{g_0} \mathbf{B}_L \mathbf{x}^{(1)} + \mathbf{F}_{g_1} \mathbf{B}_H \mathbf{z}^{(1)}, \quad (3.18)$$

where $\mathbf{B}_L := \mathbf{A}_L^\top$ and $\mathbf{B}_H := \mathbf{A}_H^\top$.

Given a signal $\mathbf{x}^{(0)}$ defined on \mathcal{G} , denote by $\mathbf{x}^{(1)}$ the output signal of the lowpass channel of the two-channel filter bank on \mathcal{G} . We equip $\mathbf{x}^{(1)}$ with a reduced graph \mathcal{G}_1 and design a new two-channel filter bank on \mathcal{G}_1 so that $\mathbf{x}^{(1)}$ can be further decomposed. The decomposition process can be implemented for several layers. The sequences of such decompositions and reconstructions, as described in (3.17) and (3.18), is illustrated in the flowchart in Table 1 and is called Mallat's algorithm.

4 Locality and Approximation Error

4.1 Locality of the Filters

4.1.1 Locality of the Filters: Theory

Different requirements lead to different design of the filter banks. In some applications, one may want the filters to be well localized in the graph domain. In the classical signal

Table 1: Mallat’s algorithms for Decomposition and Reconstruction

Decomposition	$\mathbf{x}^{(0)} \longrightarrow \mathbf{x}^{(1)} \longrightarrow \mathbf{x}^{(2)} \longrightarrow \dots$ $\searrow \mathbf{z}^{(1)} \searrow \mathbf{z}^{(2)} \searrow \dots$
Reconstruction	$\dots \longrightarrow \mathbf{x}^{(2)} \longrightarrow \mathbf{x}^{(1)} \longrightarrow \mathbf{x}^{(0)}$ $\dots \nearrow \mathbf{z}^{(2)} \nearrow \mathbf{z}^{(1)} \nearrow$

processing, the key advantage of the wavelet transform compared to the Fourier Transform is the ability of extracting both local spectral and temporal information, which makes it very applicable for processing of non-stationary signals. In the classical two-channel filter bank, wavelet transforms serve as the analysis and synthesis filters, which corresponds to the analysis and synthesis filters $\mathbf{F}_{h_0}, \mathbf{F}_{h_1}$ and $\mathbf{F}_{g_0}, \mathbf{F}_{g_1}$ in the graph settings as described in Section 2.4. Naturally, we concern about the locality of graph filters.

Let us learn from the idea in [18] to characterize the locality of a filter \mathbf{F}_h . By

$$(\mathbf{L}\mathbf{x})(i) = d_i x_i - \sum_{v_j \sim v_i} w_{ij} x_j, \quad i = 1, \dots, N,$$

where $v_j \sim v_i$ represents the edge connection between v_i and v_j , we know that $(\mathbf{L}\mathbf{x})(i)$ depends only on the values of the function \mathbf{x} on the one-hop neighborhood of v_i : $\mathcal{N}(v_i) := \{v_j | v_j \sim v_i\}$. The larger the weight w_{ij} , the greater the value $\mathbf{x}(v_j)$ contributes to $(\mathbf{L}\mathbf{x})(i)$. Similarly, $(\sum_{l=1}^k \mathbf{L}^l \mathbf{x})(i)$ only depends on the k -hop neighborhood of v_i , where the k -hop neighborhood of the vertex v_i refers to the set of vertices that can be connected to v_i by at most k edges. Therefore, if the filter \mathbf{F}_h can be written as an m -order polynomial in \mathbf{L} , then $(\mathbf{F}_h \mathbf{x})(i)$ only depends on the signal values in the m -hop neighborhood of v_i . The degree m of the polynomial can be regarded as an index of the locality of the filter \mathbf{F}_h .

We point out that the locality of graph filter $\mathbf{F}_h = p_m(\mathbf{L})$ is consistent with the locality of traditional wavelet analysis. In the traditional case, if a filter function of an orthonormal wavelet basis is a polynomial in the Fourier basis function $e^{-i\omega}$:

$$m_0(\omega) = \sum_{k=0}^m \xi_k z^k, \quad z := e^{-i\omega},$$

then the support of the scaling function ϕ and the wavelet function ψ are respectively $\text{supp}\phi \subset [0, m]$ and $\text{supp}\psi \subset [1 - m, m]$, and the Mallat’s decomposition based on this wavelet basis is [4]:

$$y_k = \sqrt{2} \sum_{l=0}^m \xi_l x_{2k+l}, \quad z_k = \sqrt{2} \sum_{l=0}^m (-1)^l \xi_l x_{2k+1-l}.$$

It can be seen that y_k and z_k depend only on the values on the vertices in the $(m+1)$ -hop neighborhood of x_{2k} .

The perfect reconstruction filters \mathbf{F}_{h_0} and \mathbf{F}_{h_1} designed according to the proposed method need to meet the conditions (3.9). It is usually difficult to find polynomials h_0, h_1, g_0, g_1 in λ such that (3.9) holds for

$$\mathbf{h}_i = (h_i(\lambda_1), \dots, h_i(\lambda_N))^\top, \quad \mathbf{g}_i = (g_i(\lambda_1), \dots, g_i(\lambda_N))^\top, \quad i = 0, 1,$$

where $\lambda_i \in \sigma(\mathbf{L})$. However, if the vectors \mathbf{h}_0 and \mathbf{h}_1 that satisfy (3.9) can be approximated by polynomials in $\lambda \in \mathbb{R}$ on $\sigma(\mathbf{L})$, then \mathbf{F}_{h_0} and \mathbf{F}_{h_1} are said to be approximately localized. This is explained by the following theorem.

Theorem 4.1. *Denote the eigenvalues of the graph Laplacian matrix \mathbf{L} by $0 = \lambda_1 \leq \dots \leq \lambda_N$. Then for any $\mathbf{h} \in \{\mathbf{h} \in \mathbb{R}^N \mid h_i = h_j \text{ if } \lambda_i = \lambda_j\}$, there exists an m -order polynomial p_m , such that*

$$\|\mathbf{F}_h - p_m(\mathbf{L})\|_2 \leq \frac{6\lambda_N}{m} M_h,$$

where M_h is the Lipschitz constant of the filter vector \mathbf{h} defined by

$$M_h := \max_{\substack{1 \leq i \leq N-1 \\ \lambda_{i+1} \neq \lambda_i}} \left| \frac{h_{i+1} - h_i}{\lambda_{i+1} - \lambda_i} \right|.$$

Proof. Suppose the eigen decomposition of \mathbf{L} is $\mathbf{L} = \mathbf{U}\Lambda\mathbf{U}^\top$, where $\Lambda := \text{diag}(\lambda_1, \dots, \lambda_N)$, then

$$\begin{aligned} \|\mathbf{F}_h - p_m(\mathbf{L})\|_2 &= \|\mathbf{U}[\text{diag}(\mathbf{h}) - p_m(\Lambda)]\mathbf{U}^\top\|_2 = \|\text{diag}(\mathbf{h}) - p_m(\Lambda)\|_2 \\ &= \max_{1 \leq i \leq N} |h_i - p_m(\lambda_i)|. \end{aligned}$$

Let f be a piecewise function connecting all the points $\{(\lambda_i, h_i)\}_{i=1}^N$ in turn, then $f \in \text{Lip}_{M_h} 1$. Namely, f is a function on $[0, \lambda_N]$ that satisfies the following Lipschitz condition:

$$|f(x) - f(y)| \leq M_h |x - y|, \quad \forall x, y \in [0, \lambda_N].$$

According to [22, Corollary 1, §6.2], there is an m -order polynomial p_m such that

$$\max_{\lambda \in [0, \lambda_N]} |f(\lambda) - p_m(\lambda)| \leq \frac{6\lambda_N}{m} M_h.$$

Since $h_i = f(\lambda_i)$, $i = 1, \dots, N$, we have $\|\mathbf{F}_h - p_m(\mathbf{L})\|_2 \leq \frac{6\lambda_N}{m} M_h$. ■

In order to construct an orthogonal filter bank $\{\mathbf{h}_0, \mathbf{g}_0, \mathbf{h}_1, \mathbf{g}_1\}$, according to Algorithm 3.1, we only need to choose $2 = y_1 \geq \dots \geq y_s \geq 1$ that satisfies (3.16). The Lipschitz constants of these filters are all equal to

$$M := \max_{\substack{1 \leq i \leq N-1 \\ \lambda_{i+1} \neq \lambda_i}} \left| \frac{\sqrt{y_i} - \sqrt{y_{i+1}}}{\Delta \lambda_i} \right|, \quad \text{with } \Delta \lambda_i := \lambda_{i+1} - \lambda_i.$$

To make $\mathbf{h}_0 = \mathbf{g}_0$ and $\mathbf{h}_1 = \mathbf{g}_1$ have as best locality as possible, by Theorem 4.1, we want the constant M to be as small as possible. When N is odd, we have $y_s = 2 - y_s$, which implies that $y_s = 1$. For simplicity, we also set $y_s = 1$ when N is even, which yields $y_{r+1} = 2 - y_s = 1$. Therefore, it always holds that $y_s = y_{r+1} = 1$ no matter N is even or odd.

For $i = 1, \dots, s-1$, let $\{\alpha_i\}$ and $\{\beta_i\}$ be nonnegative numbers satisfying

$$\begin{cases} \sqrt{y_i} - \sqrt{y_{i+1}} = \alpha_i \Delta \lambda_i, \\ \sqrt{2 - y_{i+1}} - \sqrt{2 - y_i} = \beta_i \Delta \lambda_{N-i}, \end{cases} \quad i = 1, \dots, s-1. \quad (4.1)$$

It is easy to see that $\{y_i\}_{i=1}^s$ is determined uniquely by $\{\alpha_i\}_{i=1}^{s-1}$ or $\{\beta_i\}_{i=1}^{s-1}$ given $y_1 = 2$. Summing both sides of (4.1) for i from 1 to $s-1$, we get the following constraints of $\boldsymbol{\alpha} := [\alpha_1, \dots, \alpha_{s-1}]$ and $\boldsymbol{\beta} := [\beta_1, \dots, \beta_{s-1}]$:

$$\begin{cases} \sum_{i=1}^{s-1} \alpha_i \Delta \lambda_i = \sqrt{2} - 1, \\ \boldsymbol{\alpha} \succeq \mathbf{0}, \end{cases} \quad \begin{cases} \sum_{i=1}^{s-1} \beta_i \Delta \lambda_{N-i} = 1, \\ \boldsymbol{\beta} \succeq \mathbf{0}. \end{cases} \quad (4.2)$$

Based on the constraints we propose two strategies for constructing $\boldsymbol{\alpha}$ or $\boldsymbol{\beta}$ as follows:

- Find $\boldsymbol{\alpha} \in \mathbb{R}_+^{s-1}$ which minimizes $\|\boldsymbol{\alpha}\|_\infty$ under the first constraint of (4.2).
- Find $\boldsymbol{\beta} \in \mathbb{R}_+^{s-1}$ which minimizes $\|\boldsymbol{\beta}\|_\infty$ under the second constraint of (4.2).

For the sake of simplicity, we only describe the first strategy here. The another one is similar. The minimum solution of $\|\boldsymbol{\alpha}\|_\infty$ under the first constraint of (4.2) can be obtained by the following lemma.

Lemma 4.2. *Given nonzero $\mathbf{a} = (a_1, \dots, a_n)^\top \in \mathbb{R}_+^n$ and $b \in \mathbb{R}$, if the optimization problem*

$$\min \|\mathbf{x}\|_\infty, \quad \text{s. t.} \quad \mathbf{a}^\top \mathbf{x} = b, \quad \mathbf{x} \succeq \mathbf{0} \quad (4.3)$$

has nonempty feasible set $\mathcal{D} := \{\mathbf{x} \in \mathbb{R}^n \mid \mathbf{a}^\top \mathbf{x} = b, \mathbf{x} \succeq \mathbf{0}\}$, then the optimal solution x^ exists and satisfies*

$$x_i^* = \|\mathbf{x}^*\|_\infty, \quad \forall i \in I := \{1 \leq i \leq n \mid a_i \neq 0\}. \quad (4.4)$$

Proof. Since \mathcal{D} is not an empty set, it is easy to show that the infimum of $f(\mathbf{x}) := \|\mathbf{x}\|_\infty$ on \mathcal{D} is reachable at some point $\mathbf{x}^* \in \mathcal{D}$, which is a solution of the optimization problem (4.3).

Next, let us prove (4.4) for any solution \mathbf{x}^* of (4.3).

We assume that I is not empty without losing generality. If (4.4) is not true, there must exist a $k \in I$ such that $x_k^* < \|\mathbf{x}^*\|_\infty$. For any $\epsilon > 0$, using $a_k \neq 0$ we have that

$$b = \sum_{i \in I} a_i x_i^* = a_k \left(x_k^* + a_k^{-1} \epsilon \sum_{i \in I \setminus \{k\}} a_i x_i^* \right) + \sum_{i \in I \setminus \{k\}} a_i (x_i^* - \epsilon x_i^*).$$

Define $\tilde{\mathbf{x}} := (\tilde{x}_1, \dots, \tilde{x}_n)^\top$ as follows:

$$\tilde{x}_i := \begin{cases} x_k^* + a_k^{-1} \epsilon \sum_{i \in I \setminus \{k\}} a_i x_i^* & i = k, \\ (1 - \epsilon)x_i^* & i \in I \setminus \{k\}, \\ 0 & i \notin I. \end{cases}$$

It is easy to see that, for $\epsilon > 0$ sufficiently small, there holds $\tilde{\mathbf{x}} \succeq 0$, $\mathbf{a}^\top \tilde{\mathbf{x}} = b$, and $|\tilde{x}_k| < \|\mathbf{x}^*\|_\infty$. Thus, for any $i \in I \setminus \{k\}$, we have

$$|\tilde{x}_i| = (1 - \epsilon)|x_i^*| \begin{cases} = 0 < \|\mathbf{x}^*\|_\infty & x_i^* = 0, \\ < |x_i^*| \leq \|\mathbf{x}^*\|_\infty & x_i^* \neq 0, \end{cases}$$

and consequently $\|\tilde{\mathbf{x}}\|_\infty < \|\mathbf{x}^*\|_\infty$, which contradicts the assumption that \mathbf{x}^* is an optimal solution. ■

By Lemma 4.2 we can find an $\boldsymbol{\alpha} \in \mathbb{R}_+^{s-1}$ according to the first strategy, which is

$$\alpha_1 = \dots = \alpha_{s-1} = \frac{\sqrt{2} - 1}{\sum_{i=1}^{s-1} \Delta \lambda_i} = \frac{\sqrt{2} - 1}{\lambda_s}.$$

Inserting it into (4.1), we obtain that

$$y_i = \left[\sqrt{2} - (\sqrt{2} - 1) \frac{\lambda_i}{\lambda_s} \right]^2, \quad i = 1, \dots, s. \quad (4.5)$$

Similarly, according to the second strategy we can find $\boldsymbol{\beta} \in \mathbb{R}_+^{s-1}$ as

$$\beta_1 = \dots = \beta_{s-1} = \frac{1}{\lambda_N - \lambda_{r+1}}.$$

Consequently, $\{y_i\}_{i=1}^s$ are as follows:

$$y_i = 2 - \left(\frac{\lambda_N - \lambda_{N+1-i}}{\lambda_N - \lambda_{r+1}} \right)^2, \quad i = 1, \dots, s. \quad (4.6)$$

The Lipschitz constants of the filter vector designen by the two above strategies may be different. In practical applications, we can choose the one with smaller Lipschitz constant.

To verify the above theory on the locality of the filters, let us construct the following two typical examples of perfect reconstruction orthogonal two-channel filter banks by Algorithm 3.1:

- **localFB**

$$y_i = \left[\sqrt{2} - (\sqrt{2} - 1) \frac{\lambda_i}{\lambda_s} \right]^2, \quad i = 1, \dots, s; \quad y_i = 2 - y_{N-i+1}, \quad i = s + 1, \dots, N.$$

- **idealFB**

$$y_1 = \dots = y_{s-1} = 2, \quad y_{s+1} = \dots = y_N = 0, \quad y_s = \begin{cases} 1 & \text{if } N \text{ is odd,} \\ 2 & \text{if } N \text{ is even.} \end{cases}$$

After gettingting $\{y_i\}_{i=1}^N$, we calculate filters as follows:

$$\mathbf{g}_0(i) = \mathbf{h}_0(i) = \sqrt{y_i}, \quad \mathbf{g}_1(i) = \mathbf{h}_1(i) := \mathbf{g}_0(N + 1 - i), \quad i = 1, \dots, N.$$

The localFB depends on the eigenvalues of the graph Laplacian, while the idealFB depends only on the number of vertices of the graph. Figure 4 shows the filters \mathbf{h}_0 and \mathbf{h}_1 for localFB and idealFB for the ring graph with 256 vertices.

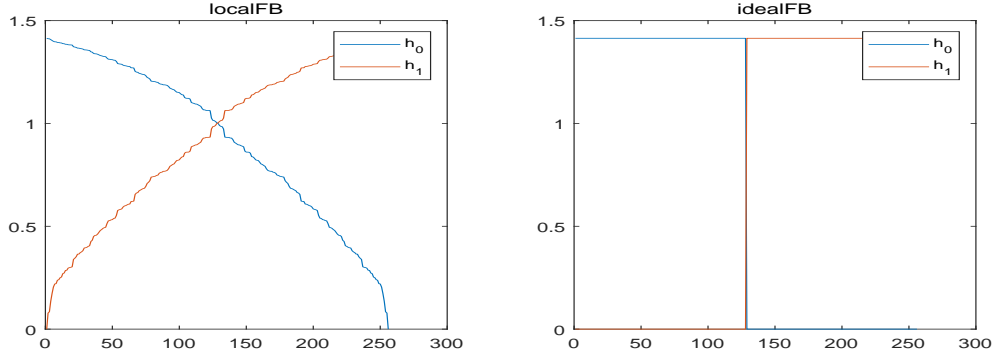


Figure 4: Two types of orthogonal filter banks constructed using the proposed method. Left: localFB, right: idealFB.

Figure 5¹ shows the filter functions $h(\lambda_i) := \mathbf{h}(i)$, $i = 1, \dots, N$ (blue color) and their uniform approximation polynomial $p_m(\lambda)$ (red color) on the ring graph (left) and the sensor graph (right) with 1000 vertices. The two filter functions on the top row are produced by the proposed localFB (the one with smaller Lipschitz constant). Their Lipschitz constants M 's are respectively 1 (ring graph) and 1.4396 (sensor graph). By the Remez algorithm [26], the corresponding 5th-order best uniform approximation polynomials are shown as the red curve. For comparison, the ideal half-band filters of idealFB and their corresponding 30th-order best uniform approximation polynomials are shown in the bottom row of the figure. The Lipschitz constants M 's, which are respectively 224.478 (ring graph) and 533.7062 (sensor graph), are much larger than those of localFB, so the ideal half-band filters cannot be well approximated uniformly by low-order polynomials.

¹Since calculating the best approximation in the uniform norm is computationally difficult, high-degree approximation polynomial for the ideal half-band filter may not be very accurate.

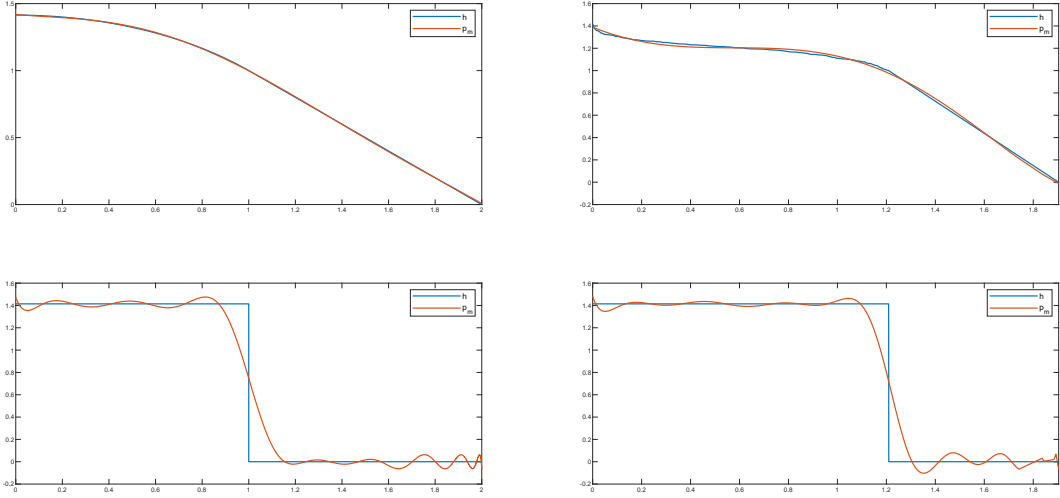


Figure 5: The top row shows the filter functions h 's designed by the proposed localFB and their 5th-order uniform approximation polynomials p_m on the ring graph (left) and on the sensor graph (right) with 1000 vertices. The bottom row correspondingly shows the ideal half-band filter functions h 's and their 30th-order uniform approximation polynomials.

4.1.2 Locality of the Filters: Experiments

In this section, we conduct experiments to verify the locality of this two types of filters: localFB and idealFB designed in 4.1.1. We consider the impulse signals on the ring graph and the community network, both have 256 vertices, and a discontinuous signal

$$\mathbf{x}(k) = 0.2 \sin\left(\frac{k-1}{2(N-1)}\pi\right), \quad k = 1, \dots, N, \quad (4.7)$$

on the ring graph with $N = 256$ vertices, which contains a step between the first vertex and the last one. The signals described above are shown in Figure 6.

We filter the above three signals with \mathbf{h}_0 (lowpass) and \mathbf{h}_1 (highpas) of localFB and idealFB and show the experimental results in Figures 7, 8 and 9. All experiments in this section and the next section are done with Matlab, and the toolbox involved is mainly GSPBox for matlab [24]. It shows that, using idealFB, the filtered signals $\mathbf{F}_{h_0}\mathbf{x}$ and $\mathbf{F}_{h_1}\mathbf{x}$ have widespread oscillations around the discontinuities, that is, samples in a wide range around the impulse/step are badly affected. In contrast, in the filtered signals of localFB, only samples in a narrow range around the impulse/step are affected. This phenomenon can be observed more clearly by enlarging the part near the step point in Figure 9, as shown in Figure 10. These experiments validate our theoretic conclusion: the filters of localFB is of much better locality in the vertex domain than those of idealFB.

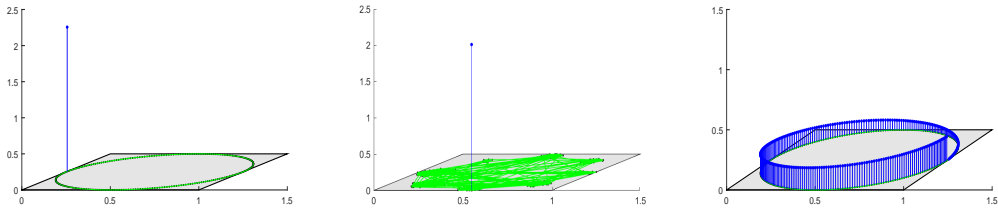


Figure 6: From left to right are the impulse signals on the ring graph, the community network of 256 vertices, and the discontinuous signal defined by (4.7) on the ring graph.

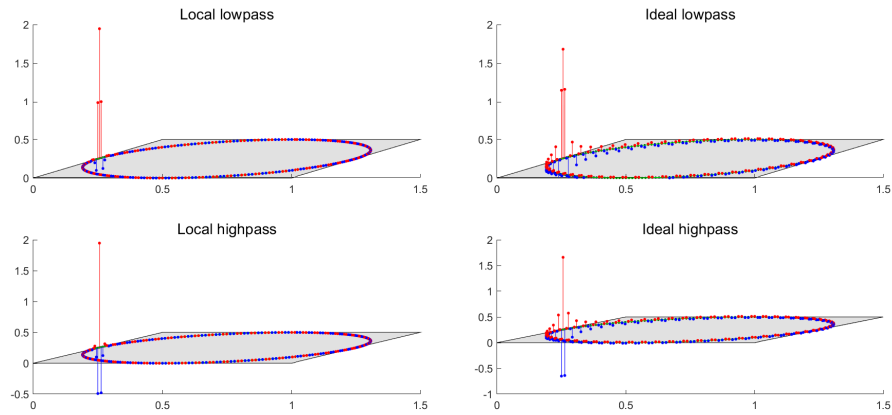


Figure 7: Filtered signals $\mathbf{F}_{h_0} \mathbf{x}$ and $\mathbf{F}_{h_1} \mathbf{x}$ for the impulse signal \mathbf{x} on the ring graph by localFB (left) and idealFB (right).

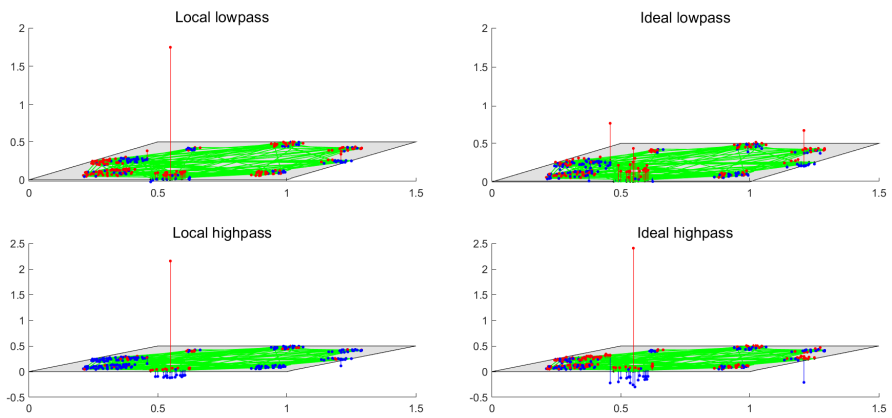


Figure 8: Filtered signals $\mathbf{F}_{h_0} \mathbf{x}$ and $\mathbf{F}_{h_1} \mathbf{x}$ for the impulse signal \mathbf{x} on the community graph by localFB (left) and idealFB (right).

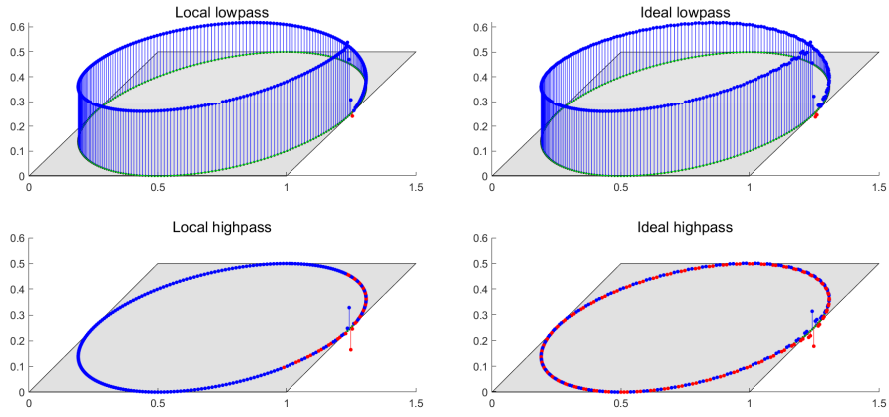


Figure 9: Filtered signals $\mathbf{F}_{h_0} \mathbf{x}$ and $\mathbf{F}_{h_1} \mathbf{x}$ for the discontinuous signal \mathbf{x} defined by (4.7) on the ring graph by localFB (left) and idealFB (right).

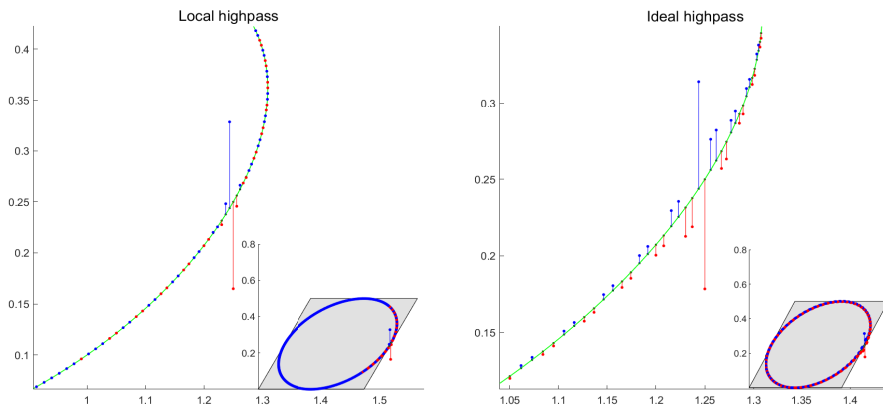


Figure 10: Partial enlargement near the step point in the figures in the bottom row of Figure 9.

4.2 Approximation Error

4.2.1 Approximation Error: Theory

For a smooth signal \mathbf{x} , it is expected that the reconstructed signal using only the output of the lowpass channel can approximate \mathbf{x} , i.e., $\mathbf{F}_{g_0} \mathbf{B}_L \mathbf{A}_L \mathbf{F}_{h_0} \mathbf{x} \approx \mathbf{x}$. By (3.2) and (3.5), we have

$$\mathbf{I}_N - \mathbf{F}_{g_0} \mathbf{B}_L \mathbf{A}_L \mathbf{F}_{h_0} = \mathbf{I}_N - \frac{1}{2} \mathbf{F}_{g_0} (\mathbf{I} + \mathbf{Q}) \mathbf{F}_{h_0} = \frac{1}{2} \mathbf{F}_{g_1} (\mathbf{I} - \mathbf{Q}) \mathbf{F}_{h_1}.$$

Since $\mathbf{F}_{h_1} \mathbf{Q} = \mathbf{Q} \mathbf{F}_{h_1 \circ \kappa}$ and \mathbf{Q} is symmetric, where $\kappa(k) = N + 1 - k$, it follows that

$$\mathbf{I}_N - \mathbf{F}_{g_0} \mathbf{B}_L \mathbf{A}_L \mathbf{F}_{h_0} = \frac{1}{2} \mathbf{F}_{g_1} (\mathbf{F}_{h_1} - \mathbf{F}_{h_1 \circ \kappa} \mathbf{Q}).$$

Therefore, for any $\mathbf{x} \in \mathbb{R}^N$, there holds

$$\begin{aligned} \mathbf{F}_{g_1} (\mathbf{F}_{h_1} - \mathbf{F}_{h_1 \circ \kappa} \mathbf{Q}) \mathbf{x} &= \mathbf{U} \text{diag}(\mathbf{g}_1) [\text{diag}(\mathbf{h}_1) \hat{\mathbf{x}} - \text{diag}(\mathbf{h}_1 \circ \kappa) \Phi \hat{\mathbf{x}}] \\ &= \mathbf{U} \text{diag}(\mathbf{g}_1) [\text{diag}(\mathbf{h}_1) \hat{\mathbf{x}} - \text{diag}(\mathbf{h}_1 \circ \kappa) (\hat{\mathbf{x}} \circ \kappa)], \end{aligned}$$

where $\Phi = \mathbf{U}^\top \mathbf{Q} \mathbf{U}$. Hence,

$$\begin{aligned} \|\mathbf{F}_{g_1} (\mathbf{F}_{h_1} - \mathbf{F}_{h_1 \circ \kappa} \mathbf{Q}) \mathbf{x}\|_2^2 &= \sum_{i=1}^N |\mathbf{g}_1(i)|^2 |\mathbf{h}_1(i) \hat{\mathbf{x}}(i) - \mathbf{h}_1(N+1-i) \hat{\mathbf{x}}(N+1-i)|^2 \\ &= \sum_{i=1}^N |\mathbf{h}_0(N+1-i)|^2 |\mathbf{g}_0(N+1-i) \hat{\mathbf{x}}(i) - \mathbf{g}_0(i) \hat{\mathbf{x}}(N+1-i)|^2. \end{aligned}$$

If N is odd, we have $s = r + 1$, $N + 1 - s = s$ and

$$|\mathbf{g}_1(s)|^2 |\mathbf{h}_1(s) \hat{\mathbf{x}}(s) - \mathbf{h}_1(N+1-s) \hat{\mathbf{x}}(N+1-s)|^2 = 0.$$

If N is even, there holds $s = r$ and the above term does not exist. In both cases we have

$$\begin{aligned} &\|\mathbf{F}_{g_1} (\mathbf{F}_{h_1} - \mathbf{F}_{h_1 \circ \kappa} \mathbf{Q}) \mathbf{x}\|_2^2 \\ &= \sum_{i=1}^r |\mathbf{h}_0(N+1-i)|^2 |\mathbf{g}_0(N+1-i) \hat{\mathbf{x}}(i) - \mathbf{g}_0(i) \hat{\mathbf{x}}(N+1-i)|^2 \\ &+ \sum_{j=1}^r |\mathbf{h}_0(j)|^2 |\mathbf{g}_0(j) \hat{\mathbf{x}}(N+1-j) - \mathbf{g}_0(N+1-j) \hat{\mathbf{x}}(j)|^2 \\ &= \sum_{i=1}^r [|\mathbf{h}_0(i)|^2 + |\mathbf{h}_0(N+1-i)|^2] |\mathbf{g}_0(N+1-i) \hat{\mathbf{x}}(i) - \mathbf{g}_0(i) \hat{\mathbf{x}}(N+1-i)|^2 \\ &= \sum_{i=1}^r |c_i(\mathbf{h}_0)|^2 |\mathbf{g}_0(N+1-i) \hat{\mathbf{x}}(i) - \mathbf{g}_0(i) \hat{\mathbf{x}}(N+1-i)|^2, \end{aligned}$$

where

$$c_i(\mathbf{h}_0) := \sqrt{|\mathbf{h}_0(i)|^2 + |\mathbf{h}_0(N+1-i)|^2}.$$

It is easy to see that $c_{N+1-i}(\mathbf{h}_0) = c_i(\mathbf{h}_0)$. If $\mathbf{g}_0(N) = 0$, using the Minkowski's inequality we obtain that

$$\begin{aligned} \|\mathbf{F}_{g_1}(\mathbf{F}_{h_1} - \mathbf{F}_{h_1 \circ \kappa} \mathbf{Q})\mathbf{x}\|_2 &\leq \left(\sum_{i=1}^r |c_i(\mathbf{h}_0) \mathbf{g}_0(N+1-i) \hat{\mathbf{x}}(i)|^2 \right)^{1/2} + \left(\sum_{i=1}^r |c_i(\mathbf{h}_0) \mathbf{g}_0(i) \hat{\mathbf{x}}(N+1-i)|^2 \right)^{1/2} \\ &\leq A_1 \sigma_1(\mathbf{x})^{1/2} + A_2 \sigma_2(\mathbf{x})^{1/2}, \end{aligned}$$

where

$$\begin{cases} \sigma_1(\mathbf{x}) := \sum_{i=1}^r \lambda_i |\hat{\mathbf{x}}(i)|^2, & A_1 := \max_{2 \leq i \leq r} \lambda_i^{-1/2} |c_i(\mathbf{h}_0) \mathbf{g}_0(N+1-i)|; \\ \sigma_2(\mathbf{x}) := \sum_{i=s+1}^N \lambda_i |\hat{\mathbf{x}}(i)|^2, & A_2 := \max_{s+1 \leq i \leq N} \lambda_i^{-1/2} |c_i(\mathbf{h}_0) \mathbf{g}_0(N+1-i)|. \end{cases} \quad (4.8)$$

Particularly, in the orthogonal case, since

$$\mathbf{g}_0(i) = \mathbf{h}_0(i) = \sqrt{\mathbf{f}(i)}, \quad \mathbf{f}(N+1-i) = 2 - \mathbf{f}(i), \quad i = 1, \dots, N,$$

we have

$$c_i(\mathbf{h}_0) := \sqrt{|\mathbf{h}_0(i)|^2 + |\mathbf{h}_0(N+1-i)|^2} = \sqrt{2},$$

and consequently

$$A_1 = \max_{2 \leq i \leq r} \sqrt{\frac{2(2 - \mathbf{f}(i))}{\lambda_i}}, \quad A_2 = \max_{s+1 \leq i \leq N} \sqrt{\frac{2(2 - \mathbf{f}(i))}{\lambda_i}}. \quad (4.9)$$

The discussion proves the following theorem on the approximation error of the lowpass channel.

Theorem 4.3. *If $\mathbf{g}_0(N) = 0$, then*

$$\|(\mathbf{I}_N - \mathbf{F}_{g_0} \mathbf{B}_L \mathbf{A}_L \mathbf{F}_{h_0})\mathbf{x}\|_2 \leq \frac{1}{2} (A_1 \sigma_1(\mathbf{x})^{1/2} + A_2 \sigma_2(\mathbf{x})^{1/2}),$$

where, $\sigma_1(\mathbf{x})$, $\sigma_2(\mathbf{x})$ and A_1, A_2 are defined by (4.8). In the orthogonal case, A_1, A_2 is also defined by (4.9).

By (2.2) we have that $\sigma_1(\mathbf{x}) + \sigma_2(\mathbf{x}) \leq S_2(\mathbf{x})$ and consequently

$$\|(\mathbf{I}_N - \mathbf{F}_{g_0} \mathbf{B}_L \mathbf{A}_L \mathbf{F}_{h_0})\mathbf{x}\|_2 \leq \frac{1}{2} \sqrt{A_1^2 + A_2^2} \sqrt{S_2(\mathbf{x})},$$

which implies that the smoother the signal the smaller the approximation error. Particularly, if \mathbf{x} is in the Paley–Wiener space $\text{PW}_r(\mathcal{G}) := \{\mathbf{x} | \hat{\mathbf{x}}(k) = 0, k > r\}$ [12], then $\sigma_2(\mathbf{x}) = 0$ and $\|(\mathbf{I}_N - \mathbf{F}_{g_0} \mathbf{B}_L \mathbf{A}_L \mathbf{F}_{h_0})\mathbf{x}\|_2 \leq \frac{1}{2} A_1 \sqrt{\sigma_1(\mathbf{x})}$. In this case the lowpass channel of idealFB gives the best approximation error 0 since $A_1 = 0$.

4.2.2 Approximation Error: Experiments

In this section, experiments are implemented to check the the approximation error of the lowpass channels of the two types of filter banks: localFB and idealFB. The experimental results are also compared with graphQMF-meyer and graphQMF-ideal proposed by Narang and Ortega in [21] and graphBior in their follow-up work [18]. We conduct experiments on the Minnesota traffic graph with normalized Laplacian, where the graph signal is the one used in [21]. All the results are shown in Figure 11: The top left is the original signal, with the color of vertices representing the signal values. One layer of decomposition is conducted, and only the lowpass-channel output is going to be used for reconstruction. Since the Minnesota traffic graph is not bipartite, the methods proposed in [21] and [18] need to decompose it into two bipartite subgraphs. Then a two-dimensional filter bank implementation is performed on these subgraphs, producing four channels: LL, LH, HL and HH channel, each channel contains 1188, 404, 0 and 1050 samples respectively. The reconstruction is done by the wavelet coefficients from LL channel only. While for methods proposed in this paper, we only have two channels: L and H channel. We only use the wavelet coefficients from L channel, containing 1321 samples, for reconstruction. We calculate the SNR and relative error (denoted as RE) of each reconstructed signal using only lowpass wavelet coefficients (denoted as reconSNR and reconRE), which are defined by

$$\text{SNR} := 10 \log_{10} \left(\frac{\|\mathbf{f}\|_2^2}{\|\mathbf{f} - \mathbf{f}_r\|_2^2} \right), \quad \text{RE} := \frac{\|\mathbf{f} - \mathbf{f}_r\|_2}{\|\mathbf{f}\|_2},$$

where \mathbf{f} is the original signal and \mathbf{f}_r is the reconstructed signal. The REs of the overall reconstruction (perfect reconstruction) of each model are also calculated (denoted as totalRE). For experiments of graphQMF and gaphBior, we use the codes provided by Narang and Ortega, see *Biorth_filterbank_demo2* and *QMF_filterbank_demo_2* in [Graph Filterbanks](#). The graphQMFs used in the experiments are based on the 24-th order polynomial approximation of meyer kernel and ideal kernel respectively. The degrees of lowpass and highpass kernels of graphBior are 16 and 17.

All the experimental results are listed in Table 2. It is easy to see that the totalRE of the two graphQMFs are much larger than the other 3 methods because they use a polynomial approximation of the kernels instead of the exact kernels. In particular, graphQMF based on the ideal kernel performs the worst because it can not be well approximated by a low-order polynomial. From Table 2, the methods proposed in this paper have perfect reconstruction and perform better in the approximation. The reconstruction signals are displayed in Figure 11.

Table 2: SNR and relative error of five different methods

	graphQMF-meyer	graphQMF-ideal	graphBior	idealFB	localFB
reconSNR	12.5647	0.9000	11.8843	15.6612	15.0422
reconRE	0.2354	0.9016	0.2546	0.1648	0.1770
totalRE	0.0030	0.8406	9.6305e-06	5.2826e-15	5.4851e-15

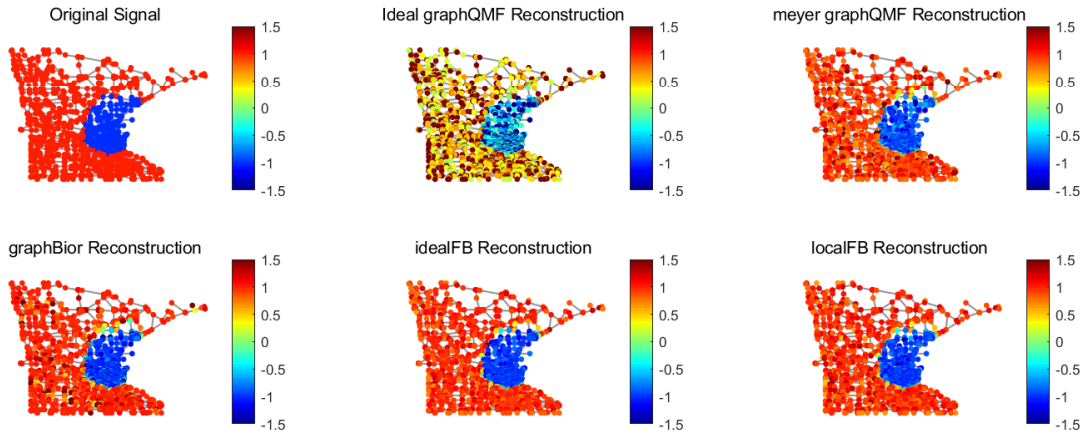


Figure 11: Reconstructed signal using only lowpass wavelet coefficients by five different methods: graphQMF-ideal (top-middle), graphQMF-meyer (top-right), graphBior (bottom-left), idealFB (bottom-middle) and localFB (bottom-right). The top-left is the original signal.

References

- [1] Fan RK Chung and Fan Chung Graham. *Spectral graph theory*. American Mathematical Soc., 1997.
- [2] Ronald R Coifman and Mauro Maggioni. Diffusion wavelets. *Applied and Computational Harmonic Analysis*, 21(1):53–94, 2006.
- [3] Mark Crovella and Eric Kolaczyk. Graph wavelets for spatial traffic analysis. In *IEEE INFOCOM 2003. Twenty-second Annual Joint Conference of the IEEE Computer and Communications Societies (IEEE Cat. No. 03CH37428)*, volume 3, pages 1848–1857. IEEE, 2003.
- [4] Ingrid Daubechies. *Ten lectures on wavelets*. SIAM, 1992.
- [5] Joya A Deri and José MF Moura. Spectral projector-based graph fourier transforms. *IEEE Journal of Selected Topics in Signal Processing*, 11(6):785–795, 2017.
- [6] Bin Dong. Sparse representation on graphs by tight wavelet frames and applications. *Applied and Computational Harmonic Analysis*, 42(3):452–479, 2017.
- [7] Florian Dorfler and Francesco Bullo. Kron reduction of graphs with applications to electrical networks. *IEEE Transactions on Circuits and Systems I: Regular Papers*, 60(1):150–163, 2012.
- [8] Venkatesan N Ekambaram, Giulia C Fanti, Babak Ayazifar, and Kannan Ramchandran. Spline-like wavelet filterbanks for multiresolution analysis of graph-structured data. *IEEE Transactions on Signal and Information Processing over Networks*, 1(4):268–278, 2015.
- [9] Matan Gavish, Boaz Nadler, and Ronald R Coifman. Multiscale wavelets on trees, graphs and high dimensional data: Theory and applications to semi supervised learning. In *ICML*, 2010.
- [10] David K Hammond, Pierre Vandergheynst, and Rémi Gribonval. Wavelets on graphs via spectral graph theory. *Applied and Computational Harmonic Analysis*, 30(2):129–150, 2011.
- [11] Chao Huang, Qian Zhang, Jianfeng Huang, and Lihua Yang. Reconstruction of bandlimited graph signals from measurements. *Digital Signal Processing*, 101:102728, 2020.
- [12] Chao Huang, Qian Zhang, Jianfeng Huang, and Lihua Yang. Approximation theorems on graphs. *Journal of Approximation Theory*, 270:105620, 2021.

- [13] Ireneusz Jabłoński. Graph signal processing in applications to sensor networks, smart grids, and smart cities. *IEEE Sensors Journal*, 17(23):7659–7666, 2017.
- [14] Madeleine S Kotzagiannidis and Pier Luigi Dragotti. Splines and wavelets on circulant graphs. *Applied and Computational Harmonic Analysis*, 47(2):481–515, 2019.
- [15] Wuhong Lin, Jianfeng Huang, Ching Yee Suen, and Lihua Yang. A feature extraction model based on discriminative graph signals. *Expert Systems with Applications*, 139:112861, 2020.
- [16] Andreas Loukas. Graph reduction with spectral and cut guarantees. *J. Mach. Learn. Res.*, 20(116):1–42, 2019.
- [17] Kenji Nakahira and Atsushi Miyamoto. Parseval wavelets on hierarchical graphs. *Applied and Computational Harmonic Analysis*, 44(2):414–445, 2018.
- [18] Narang, S.K, Ortega, and A. Compact support biorthogonal wavelet filterbanks for arbitrary undirected graphs. *IEEE Transactions on Signal Processing*, 61(19):4673–4685, 2013.
- [19] Sunil K Narang, Akshay Gadde, Eduard Sanou, and Antonio Ortega. Localized iterative methods for interpolation in graph structured data. In *2013 IEEE Global Conference on Signal and Information Processing*, pages 491–494. IEEE, 2013.
- [20] Sunil K Narang and Antonio Ortega. Local two-channel critically sampled filter-banks on graphs. In *2010 IEEE International Conference on Image Processing*, pages 333–336. IEEE, 2010.
- [21] Sunil K Narang and Antonio Ortega. Perfect reconstruction two-channel wavelet filter banks for graph structured data. *IEEE Transactions on Signal Processing*, 60(6):2786–2799, 2012.
- [22] Isidor Pavlovich Natanson. *Constructive theory of functions*, volume 1. US Atomic Energy Commission, Office of Technical Information Extension, 1961.
- [23] Antonio Ortega, Pascal Frossard, Jelena Kovačević, José MF Moura, and Pierre Vandergheynst. Graph signal processing: Overview, challenges, and applications. *Proceedings of the IEEE*, 106(5):808–828, 2018.
- [24] Nathanaël Perraudin, Johan Paratte, David Shuman, Lionel Martin, Vassilis Kalofolias, Pierre Vandergheynst, and David K Hammond. Gspbox: A toolbox for signal processing on graphs. *arXiv preprint arXiv:1408.5781*, 2014.
- [25] Isaac Z Pesenson and Meyer Z Pesenson. Sampling, filtering and sparse approximations on combinatorial graphs. *Journal of Fourier Analysis and Applications*, 16(6):921–942, 2010.

- [26] Eugene Remes. Sur le calcul effectif des polynomes d’approximation de tchebichef. *CR Acad. Sci. Paris*, 199:337–340, 1934.
- [27] Dorit Ron, Ilya Safro, and Achi Brandt. Relaxation-based coarsening and multiscale graph organization. *Multiscale Modeling & Simulation*, 9(1):407–423, 2011.
- [28] Ilya Safro, Peter Sanders, and Christian Schulz. Advanced coarsening schemes for graph partitioning. *Journal of Experimental Algorithmics (JEA)*, 19:1–24, 2015.
- [29] Peter Sanders and Christian Schulz. Engineering multilevel graph partitioning algorithms. In *European Symposium on Algorithms*, pages 469–480. Springer, 2011.
- [30] Aliaksei Sandryhaila and José MF Moura. Discrete signal processing on graphs: Graph fourier transform. In *2013 IEEE International Conference on Acoustics, Speech and Signal Processing*, pages 6167–6170. IEEE, 2013.
- [31] Aliaksei Sandryhaila and Jose MF Moura. Big data analysis with signal processing on graphs: Representation and processing of massive data sets with irregular structure. *IEEE Signal Processing Magazine*, 31(5):80–90, 2014.
- [32] David I Shuman, Mohammad Javad Faraji, and Pierre Vandergheynst. A multi-scale pyramid transform for graph signals. *IEEE Transactions on Signal Processing*, 64(8):2119–2134, 2015.
- [33] David I Shuman, Sunil K Narang, Pascal Frossard, Antonio Ortega, and Pierre Vandergheynst. The emerging field of signal processing on graphs: Extending high-dimensional data analysis to networks and other irregular domains. *IEEE signal processing magazine*, 30(3):83–98, 2013.
- [34] David I Shuman, Christoph Wiesmeyr, Nicki Holighaus, and Pierre Vandergheynst. Spectrum-adapted tight graph wavelet and vertex-frequency frames. *IEEE Transactions on Signal Processing*, 63(16):4223–4235, 2015.
- [35] David BH Tay, Yuichi Tanaka, and Akie Sakiyama. Almost tight spectral graph wavelets with polynomial filters. *IEEE Journal of Selected Topics in Signal Processing*, 11(6):812–824, 2017.
- [36] Martin Vetterli and Jelena Kovacevic. *Wavelets and subband coding*. Prentice-hall, 1995.
- [37] Joab R Winkler. *Orthogonal wavelets via filter banks: Theory and applications*. 2000.
- [38] Guangrui Yang, Lihua Yang, and Chao Huang. An orthogonal partition selection strategy for the sampling of graph signals with successive local aggregations. *Signal Processing*, page 108211, 2021.

- [39] Guangrui Yang, Lihua Yang, Zhihua Yang, and Chao Huang. Efficient node selection strategy for sampling bandlimited signals on graphs. *IEEE Transactions on Signal Processing*, 2021.
- [40] Lihua Yang, Anna Qi, Chao Huang, and Jianfeng Huang. Graph Fourier transform based on ℓ_1 norm variation minimization. *Applied and Computational Harmonic Analysis*, 52:348–365, 2021.
- [41] Zhihua Yang, Feng Zhou, Lihua Yang, and Qian Zhang. A new prediction method for recommendation system based on sampling reconstruction of signal on graph. *Expert Systems with Applications*, 159:113587, 2020.